

Finite temperature correlations and density profiles of an inhomogeneous interacting 1D Bose gas

K. V. Khenuntsyan,¹ D. M. Gangardt,^{2,3} P. D. Drummond,¹ and G. V. Shlyapnikov^{2,4}

¹ARC Centre of Excellence for Quantum Atom Optics, Department of Physics,
University of Queensland, Brisbane, Qld 4072, Australia

²Laboratoire de Physique Theorique et Modeles Statistiques,
Universite Paris Sud, 91405 Orsay Cedex, France

³Laboratoire Kastler-Brossel, Ecole Normale Supérieure, 24 rue Lhomond, 75005 Paris, France

⁴Van der Waals - Zeeman Institute, University of Amsterdam,
Valckenierstraat 65/67, 1018 XE Amsterdam, The Netherlands

(Dated: April 14, 2024)

We calculate the density profiles and density correlation functions of the one-dimensional Bose gas in a harmonic trap, using the exact finite-temperature solutions for the uniform case, and applying a local density approximation. The results are valid for a trapping potential which is slowly varying relative to a correlation length. They allow a direct experimental test of the transition from the weak coupling Gross-Pitaevskii regime to the strong coupling, 'Fermionic' Tonks-Girardeau regime. We also calculate the average two-particle correlation which characterizes the bulk properties of the sample, and find that it can be well approximated by the value of the local pair correlation in the trap center.

PACS numbers: 05.30.Jp, 03.75.Hh, 03.75.Pp

I. INTRODUCTION

The simplest investigations into a many-body system like a Bose-Einstein condensate comprise studies of thermal equilibrium properties, and the physics of small fluctuations around thermal equilibrium. For one-dimensional systems, very similar behavior is found using either photons in optical fibres or ultra-cold atoms in waveguides. Although techniques are not yet as experimentally advanced in the latter case, preliminary theory and some experimental measurements have already taken place. The atomic systems have the advantage that relatively long interaction times, large interaction strengths and low losses are possible, thus potentially allowing stringent tests of underlying quantum correlations. In this paper, we extend previous studies of correlations to include the experimentally realistic case of atoms in a waveguide with a harmonic longitudinal confining potential. The treatment is at finite temperature, and makes use of exact results for the uniform gas, together with a local density approximation.

For strong radial confinement, these types of system are examples of one-dimensional quantum (1D) gases [1, 2, 3, 4, 5]. They have the important property that in many cases their energy eigenstates are exactly solvable [6, 7, 8, 9, 10, 11, 12, 13], resulting in a greatly increased fundamental understanding of the relevant quantum field theory. For this reason, the study of 1D systems plays an important role in the physics of quantum many-body systems. It is possible to make first-principle predictions without introducing added approximations like perturbation theory. This permits direct experimental tests of the underlying many-body quantum physics, as has been demonstrated in photonics with squeezed solitons in optical fibres [14].

For ultra-cold atomic systems with repulsive interactions, the most interesting and exciting feature is the predicted transition of an interacting gas of bosons to a 'Fermionized' Tonks-Girardeau [6] regime at large coupling strengths and low densities.

We have recently made use of the known exact solutions to the uniform one-dimensional (1D) interacting Bose gas problem to calculate the exact local second-order correlation function at all densities and interaction strengths [15, 16, 17]. This is the most direct indication of 'Fermionic' behaviour, since this correlation function is strongly reduced at low density and strong coupling (similar to the case of fermions, where it vanishes exactly, due to the Pauli exclusion principle).

The first experimental evidence of reduced or 'anti-bunched' correlations in a 1D Bose gas has recently been demonstrated in Ref. [3]. However, current experiments typically take place in traps, with a longitudinal trapping potential. Provided the trap potential varies slowly, this environment is sufficiently close to a uniform one so that the exact solutions can still be used locally, in an approximation called the local density approximation.

In this paper, we make use of the local density approximation (LDA) to calculate the density profile and finite temperature local pair correlation function of a 1D Bose gas trapped in a harmonic potential. The results are valid for sufficiently low longitudinal trap frequencies, and make use of the exact solutions to the plane-wave Lieb-Liniger model [7] at finite temperature, together with the Hellmann-Feynman theorem. We mostly focus on regimes with quantum degeneracy. This requires temperatures $T < T_0$, where $T_0 = N^{-1} \lambda_z$ is the temperature of quantum degeneracy of the trapped sample as a whole, N is the total number of particles, and λ_z is the axial trap frequency.

Our main results show how 'Fermionization' can be readily detected through a simple measurement of the pair correlation averaged over the trap. This is very close to the correlation at the trap center as predicted [16] using the Lieb-Liniger uniform model, and in principle can be measured via photoassociation of trapped atoms, or other related two-body inelastic processes whose rates are governed by the local pair correlations [18]. In addition, an indirect measure of the pair correlations can be obtained [15, 19] via the measurement of three-body recombination rates as recently demonstrated experimentally [3].

II. ONE-DIMENSIONAL BOSE GAS

One dimensional quantum field theories have the important and useful property that they are often exactly solvable. This is not generally the case for higher-dimensional quantum field theories. Thus, the study of these 1D models can lead to an insight into the nature of quantum field theory for interacting particles, that is not possible from the usual perturbative approaches. In this section, we review the physics of these exact solutions for interacting bosons in the uniform 1D case, and introduce the theoretical framework for treating a non-uniform gas within the local density approximation.

A. Hamiltonian

The study of exact solutions for the one-dimensional Bose gas started with Girardeau's seminal work [6] on hard-core, or impenetrable bosons. In this model, there is a remarkable and exact correspondence between the measurable correlation functions of free fermions, and those of strongly interacting bosons. In the 1D Bose gas model with a delta-function interaction, solved by Lieb and Liniger [7], the particles can pass through each other, so they are no longer impenetrable. This provides a realistic description of a wave-guide with transverse dimensions larger than the 'core' of a particle in the wave-guide. Under these circumstances, there may only be a single relevant transverse mode, yet particles are able to exchange their positions as they propagate past each other.

Thus, we start by reviewing the theory of a gas of N bosons interacting via a delta-function potential in one dimension. The 1D Bose gas has a short-range repulsive interaction between particles which is characterized by just one coupling constant. In second quantization, the Hamiltonian is

$$\hat{H} = \frac{\hbar^2}{2m} \int_{-\infty}^{\infty} dz \partial_z \hat{\psi}^\dagger \partial_z \hat{\psi} + \frac{g}{2} \int_{-\infty}^{\infty} dz \hat{\psi}^\dagger \hat{\psi}^\dagger \hat{\psi} \hat{\psi} + \int_{-\infty}^{\infty} dz V(z) \hat{\psi}^\dagger \hat{\psi}; \quad (2.1)$$

where $\hat{\psi}(z)$ is the bosonic field operator, m is the atom mass, $g > 0$ is the coupling constant, and $V(z)$ is the trapping potential which we assume is harmonic with $V(z) = \frac{1}{2} m \omega_z^2 z^2$, while ω_z is the trap oscillation frequency in the axial direction. To treat the uniform gas we set $V(z) = 0$.

For Bose gases in highly elongated cylindrical traps ($\omega_z \ll \omega_\perp$, where ω_\perp is the frequency of the transverse harmonic potential) such that the sample can be described by the above 1D model, the coupling constant g is expressed through the 3D scattering length a [20]. For a positive scattering length a which is much smaller than the amplitude of transverse (x, y -direction) zero point oscillations, or the transverse harmonic oscillator length,

$$l_\perp = \sqrt{\frac{\hbar}{m \omega_\perp}}; \quad (2.2)$$

one has

$$g = \frac{2\hbar^2 a}{m l_\perp^2} = 2\omega_\perp a; \quad (2.3)$$

The 1D regime is reached if l_\perp is much smaller than the thermal de Broglie wavelength $\lambda_T = (2\hbar^2/mT)^{1/2}$ and a characteristic length scale l_c [21] responsible for short-range correlations. On the same grounds as at $T = 0$ [15], one finds that for fulfilling this requirement it is sufficient to satisfy the inequalities

$$a \ll l_\perp \ll \lambda_T; \quad (2.4)$$

where $n(0) = \langle \hat{\psi}^\dagger(0) \hat{\psi}(0) \rangle$ is the 1D (linear) density in the center of the trap, $z = 0$.

B. Ground-state solution for the uniform gas

We now give a brief overview of the uniform ($V(z) = 0$) Bose gas problem describing a gas of N bosons interacting via a pairwise repulsive delta-function potential in a 1D box of length L with periodic boundary condition [7]. In the thermodynamic limit ($N, L \rightarrow \infty$, while the 1D linear density $n = N/L$ is kept constant), the solution to the energy eigenstates is found [7] using the Bethe ansatz [22]. In this solution, all relative wave-functions are assumed to have a plane-wave form (except for finite changes in gradient at each collision where two particle coordinates are equal:

$$\Psi_N = \sum_{i=1}^N \sum_{j>i}^N \int \prod_{k=1}^N \frac{d^3 k_k}{(2\pi)^3} e^{i \sum_{k=1}^N \mathbf{k}_k \cdot \mathbf{r}_k} \prod_{i=1}^N \int \frac{d^3 p_i}{(2\pi)^3} e^{i \mathbf{p}_i \cdot \mathbf{r}_i} \prod_{i=1}^N \int \frac{d^3 q_i}{(2\pi)^3} e^{i \mathbf{q}_i \cdot \mathbf{r}_i} \prod_{i=1}^N \int \frac{d^3 r_i}{(2\pi)^3} e^{i \mathbf{r}_i \cdot \mathbf{r}_i} \prod_{i=1}^N \int \frac{d^3 s_i}{(2\pi)^3} e^{i \mathbf{s}_i \cdot \mathbf{r}_i} \prod_{i=1}^N \int \frac{d^3 t_i}{(2\pi)^3} e^{i \mathbf{t}_i \cdot \mathbf{r}_i} \prod_{i=1}^N \int \frac{d^3 u_i}{(2\pi)^3} e^{i \mathbf{u}_i \cdot \mathbf{r}_i} \prod_{i=1}^N \int \frac{d^3 v_i}{(2\pi)^3} e^{i \mathbf{v}_i \cdot \mathbf{r}_i} \prod_{i=1}^N \int \frac{d^3 w_i}{(2\pi)^3} e^{i \mathbf{w}_i \cdot \mathbf{r}_i} \prod_{i=1}^N \int \frac{d^3 x_i}{(2\pi)^3} e^{i \mathbf{x}_i \cdot \mathbf{r}_i} \prod_{i=1}^N \int \frac{d^3 y_i}{(2\pi)^3} e^{i \mathbf{y}_i \cdot \mathbf{r}_i} \prod_{i=1}^N \int \frac{d^3 z_i}{(2\pi)^3} e^{i \mathbf{z}_i \cdot \mathbf{r}_i} \prod_{i=1}^N \int \frac{d^3 \alpha_i}{(2\pi)^3} e^{i \mathbf{\alpha}_i \cdot \mathbf{r}_i} \prod_{i=1}^N \int \frac{d^3 \beta_i}{(2\pi)^3} e^{i \mathbf{\beta}_i \cdot \mathbf{r}_i} \prod_{i=1}^N \int \frac{d^3 \gamma_i}{(2\pi)^3} e^{i \mathbf{\gamma}_i \cdot \mathbf{r}_i} \prod_{i=1}^N \int \frac{d^3 \delta_i}{(2\pi)^3} e^{i \mathbf{\delta}_i \cdot \mathbf{r}_i} \prod_{i=1}^N \int \frac{d^3 \epsilon_i}{(2\pi)^3} e^{i \mathbf{\epsilon}_i \cdot \mathbf{r}_i} \prod_{i=1}^N \int \frac{d^3 \zeta_i}{(2\pi)^3} e^{i \mathbf{\zeta}_i \cdot \mathbf{r}_i} \prod_{i=1}^N \int \frac{d^3 \eta_i}{(2\pi)^3} e^{i \mathbf{\eta}_i \cdot \mathbf{r}_i} \prod_{i=1}^N \int \frac{d^3 \theta_i}{(2\pi)^3} e^{i \mathbf{\theta}_i \cdot \mathbf{r}_i} \prod_{i=1}^N \int \frac{d^3 \iota_i}{(2\pi)^3} e^{i \mathbf{\iota}_i \cdot \mathbf{r}_i} \prod_{i=1}^N \int \frac{d^3 \kappa_i}{(2\pi)^3} e^{i \mathbf{\kappa}_i \cdot \mathbf{r}_i} \prod_{i=1}^N \int \frac{d^3 \lambda_i}{(2\pi)^3} e^{i \mathbf{\lambda}_i \cdot \mathbf{r}_i} \prod_{i=1}^N \int \frac{d^3 \mu_i}{(2\pi)^3} e^{i \mathbf{\mu}_i \cdot \mathbf{r}_i} \prod_{i=1}^N \int \frac{d^3 \nu_i}{(2\pi)^3} e^{i \mathbf{\nu}_i \cdot \mathbf{r}_i} \prod_{i=1}^N \int \frac{d^3 \xi_i}{(2\pi)^3} e^{i \mathbf{\xi}_i \cdot \mathbf{r}_i} \prod_{i=1}^N \int \frac{d^3 \omicron_i}{(2\pi)^3} e^{i \mathbf{\omicron}_i \cdot \mathbf{r}_i} \prod_{i=1}^N \int \frac{d^3 \pi_i}{(2\pi)^3} e^{i \mathbf{\pi}_i \cdot \mathbf{r}_i} \prod_{i=1}^N \int \frac{d^3 \rho_i}{(2\pi)^3} e^{i \mathbf{\rho}_i \cdot \mathbf{r}_i} \prod_{i=1}^N \int \frac{d^3 \sigma_i}{(2\pi)^3} e^{i \mathbf{\sigma}_i \cdot \mathbf{r}_i} \prod_{i=1}^N \int \frac{d^3 \tau_i}{(2\pi)^3} e^{i \mathbf{\tau}_i \cdot \mathbf{r}_i} \prod_{i=1}^N \int \frac{d^3 \upsilon_i}{(2\pi)^3} e^{i \mathbf{\upsilon}_i \cdot \mathbf{r}_i} \prod_{i=1}^N \int \frac{d^3 \phi_i}{(2\pi)^3} e^{i \mathbf{\phi}_i \cdot \mathbf{r}_i} \prod_{i=1}^N \int \frac{d^3 \chi_i}{(2\pi)^3} e^{i \mathbf{\chi}_i \cdot \mathbf{r}_i} \prod_{i=1}^N \int \frac{d^3 \psi_i}{(2\pi)^3} e^{i \mathbf{\psi}_i \cdot \mathbf{r}_i} \prod_{i=1}^N \int \frac{d^3 \omega_i}{(2\pi)^3} e^{i \mathbf{\omega}_i \cdot \mathbf{r}_i} \prod_{i=1}^N \int \frac{d^3 \delta_i}{(2\pi)^3} e^{i \mathbf{\delta}_i \cdot \mathbf{r}_i} \prod_{i=1}^N \int \frac{d^3 \epsilon_i}{(2\pi)^3} e^{i \mathbf{\epsilon}_i \cdot \mathbf{r}_i} \prod_{i=1}^N \int \frac{d^3 \zeta_i}{(2\pi)^3} e^{i \mathbf{\zeta}_i \cdot \mathbf{r}_i} \prod_{i=1}^N \int \frac{d^3 \eta_i}{(2\pi)^3} e^{i \mathbf{\eta}_i \cdot \mathbf{r}_i} \prod_{i=1}^N \int \frac{d^3 \theta_i}{(2\pi)^3} e^{i \mathbf{\theta}_i \cdot \mathbf{r}_i} \prod_{i=1}^N \int \frac{d^3 \iota_i}{(2\pi)^3} e^{i \mathbf{\iota}_i \cdot \mathbf{r}_i} \prod_{i=1}^N \int \frac{d^3 \kappa_i}{(2\pi)^3} e^{i \mathbf{\kappa}_i \cdot \mathbf{r}_i} \prod_{i=1}^N \int \frac{d^3 \lambda_i}{(2\pi)^3} e^{i \mathbf{\lambda}_i \cdot \mathbf{r}_i} \prod_{i=1}^N \int \frac{d^3 \mu_i}{(2\pi)^3} e^{i \mathbf{\mu}_i \cdot \mathbf{r}_i} \prod_{i=1}^N \int \frac{d^3 \nu_i}{(2\pi)^3} e^{i \mathbf{\nu}_i \cdot \mathbf{r}_i} \prod_{i=1}^N \int \frac{d^3 \xi_i}{(2\pi)^3} e^{i \mathbf{\xi}_i \cdot \mathbf{r}_i} \prod_{i=1}^N \int \frac{d^3 \omicron_i}{(2\pi)^3} e^{i \mathbf{\omicron}_i \cdot \mathbf{r}_i} \prod_{i=1}^N \int \frac{d^3 \pi_i}{(2\pi)^3} e^{i \mathbf{\pi}_i \cdot \mathbf{r}_i} \prod_{i=1}^N \int \frac{d^3 \rho_i}{(2\pi)^3} e^{i \mathbf{\rho}_i \cdot \mathbf{r}_i} \prod_{i=1}^N \int \frac{d^3 \sigma_i}{(2\pi)^3} e^{i \mathbf{\sigma}_i \cdot \mathbf{r}_i} \prod_{i=1}^N \int \frac{d^3 \tau_i}{(2\pi)^3} e^{i \mathbf{\tau}_i \cdot \mathbf{r}_i} \prod_{i=1}^N \int \frac{d^3 \upsilon_i}{(2\pi)^3} e^{i \mathbf{\upsilon}_i \cdot \mathbf{r}_i} \prod_{i=1}^N \int \frac{d^3 \phi_i}{(2\pi)^3} e^{i \mathbf{\phi}_i \cdot \mathbf{r}_i} \prod_{i=1}^N \int \frac{d^3 \chi_i}{(2\pi)^3} e^{i \mathbf{\chi}_i \cdot \mathbf{r}_i} \prod_{i=1}^N \int \frac{d^3 \psi_i}{(2\pi)^3} e^{i \mathbf{\psi}_i \cdot \mathbf{r}_i} \prod_{i=1}^N \int \frac{d^3 \omega_i}{(2\pi)^3} e^{i \mathbf{\omega}_i \cdot \mathbf{r}_i} \prod_{i=1}^N \int \frac{d^3 \delta_i}{(2\pi)^3} e^{i \mathbf{\delta}_i \cdot \mathbf{r}_i} \prod_{i=1}^N \int \frac{d^3 \epsilon_i}{(2\pi)^3} e^{i \mathbf{\epsilon}_i \cdot \mathbf{r}_i} \prod_{i=1}^N \int \frac{d^3 \zeta_i}{(2\pi)^3} e^{i \mathbf{\zeta}_i \cdot \mathbf{r}_i} \prod_{i=1}^N \int \frac{d^3 \eta_i}{(2\pi)^3} e^{i \mathbf{\eta}_i \cdot \mathbf{r}_i} \prod_{i=1}^N \int \frac{d^3 \theta_i}{(2\pi)^3} e^{i \mathbf{\theta}_i \cdot \mathbf{r}_i} \prod_{i=1}^N \int \frac{d^3 \iota_i}{(2\pi)^3} e^{i \mathbf{\iota}_i \cdot \mathbf{r}_i} \prod_{i=1}^N \int \frac{d^3 \kappa_i}{(2\pi)^3} e^{i \mathbf{\kappa}_i \cdot \mathbf{r}_i} \prod_{i=1}^N \int \frac{d^3 \lambda_i}{(2\pi)^3} e^{i \mathbf{\lambda}_i \cdot \mathbf{r}_i} \prod_{i=1}^N \int \frac{d^3 \mu_i}{(2\pi)^3} e^{i \mathbf{\mu}_i \cdot \mathbf{r}_i} \prod_{i=1}^N \int \frac{d^3 \nu_i}{(2\pi)^3} e^{i \mathbf{\nu}_i \cdot \mathbf{r}_i} \prod_{i=1}^N \int \frac{d^3 \xi_i}{(2\pi)^3} e^{i \mathbf{\xi}_i \cdot \mathbf{r}_i} \prod_{i=1}^N \int \frac{d^3 \omicron_i}{(2\pi)^3} e^{i \mathbf{\omicron}_i \cdot \mathbf{r}_i} \prod_{i=1}^N \int \frac{d^3 \pi_i}{(2\pi)^3} e^{i \mathbf{\pi}_i \cdot \mathbf{r}_i} \prod_{i=1}^N \int \frac{d^3 \rho_i}{(2\pi)^3} e^{i \mathbf{\rho}_i \cdot \mathbf{r}_i} \prod_{i=1}^N \int \frac{d^3 \sigma_i}{(2\pi)^3} e^{i \mathbf{\sigma}_i \cdot \mathbf{r}_i} \prod_{i=1}^N \int \frac{d^3 \tau_i}{(2\pi)^3} e^{i \mathbf{\tau}_i \cdot \mathbf{r}_i} \prod_{i=1}^N \int \frac{d^3 \upsilon_i}{(2\pi)^3} e^{i \mathbf{\upsilon}_i \cdot \mathbf{r}_i} \prod_{i=1}^N \int \frac{d^3 \phi_i}{(2\pi)^3} e^{i \mathbf{\phi}_i \cdot \mathbf{r}_i} \prod_{i=1}^N \int \frac{d^3 \chi_i}{(2\pi)^3} e^{i \mathbf{\chi}_i \cdot \mathbf{r}_i} \prod_{i=1}^N \int \frac{d^3 \psi_i}{(2\pi)^3} e^{i \mathbf{\psi}_i \cdot \mathbf{r}_i} \prod_{i=1}^N \int \frac{d^3 \omega_i}{(2\pi)^3} e^{i \mathbf{\omega}_i \cdot \mathbf{r}_i} \prod_{i=1}^N \int \frac{d^3 \delta_i}{(2\pi)^3} e^{i \mathbf{\delta}_i \cdot \mathbf{r}_i} \prod_{i=1}^N \int \frac{d^3 \epsilon_i}{(2\pi)^3} e^{i \mathbf{\epsilon}_i \cdot \mathbf{r}_i} \prod_{i=1}^N \int \frac{d^3 \zeta_i}{(2\pi)^3} e^{i \mathbf{\zeta}_i \cdot \mathbf{r}_i} \prod_{i=1}^N \int \frac{d^3 \eta_i}{(2\pi)^3} e^{i \mathbf{\eta}_i \cdot \mathbf{r}_i} \prod_{i=1}^N \int \frac{d^3 \theta_i}{(2\pi)^3} e^{i \mathbf{\theta}_i \cdot \mathbf{r}_i} \prod_{i=1}^N \int \frac{d^3 \iota_i}{(2\pi)^3} e^{i \mathbf{\iota}_i \cdot \mathbf{r}_i} \prod_{i=1}^N \int \frac{d^3 \kappa_i}{(2\pi)^3} e^{i \mathbf{\kappa}_i \cdot \mathbf{r}_i} \prod_{i=1}^N \int \frac{d^3 \lambda_i}{(2\pi)^3} e^{i \mathbf{\lambda}_i \cdot \mathbf{r}_i} \prod_{i=1}^N \int \frac{d^3 \mu_i}{(2\pi)^3} e^{i \mathbf{\mu}_i \cdot \mathbf{r}_i} \prod_{i=1}^N \int \frac{d^3 \nu_i}{(2\pi)^3} e^{i \mathbf{\nu}_i \cdot \mathbf{r}_i} \prod_{i=1}^N \int \frac{d^3 \xi_i}{(2\pi)^3} e^{i \mathbf{\xi}_i \cdot \mathbf{r}_i} \prod_{i=1}^N \int \frac{d^3 \omicron_i}{(2\pi)^3} e^{i \mathbf{\omicron}_i \cdot \mathbf{r}_i} \prod_{i=1}^N \int \frac{d^3 \pi_i}{(2\pi)^3} e^{i \mathbf{\pi}_i \cdot \mathbf{r}_i} \prod_{i=1}^N \int \frac{d^3 \rho_i}{(2\pi)^3} e^{i \mathbf{\rho}_i \cdot \mathbf{r}_i} \prod_{i=1}^N \int \frac{d^3 \sigma_i}{(2\pi)^3} e^{i \mathbf{\sigma}_i \cdot \mathbf{r}_i} \prod_{i=1}^N \int \frac{d^3 \tau_i}{(2\pi)^3} e^{i \mathbf{\tau}_i \cdot \mathbf{r}_i} \prod_{i=1}^N \int \frac{d^3 \upsilon_i}{(2\pi)^3} e^{i \mathbf{\upsilon}_i \cdot \mathbf{r}_i} \prod_{i=1}^N \int \frac{d^3 \phi_i}{(2\pi)^3} e^{i \mathbf{\phi}_i \cdot \mathbf{r}_i} \prod_{i=1}^N \int \frac{d^3 \chi_i}{(2\pi)^3} e^{i \mathbf{\chi}_i \cdot \mathbf{r}_i} \prod_{i=1}^N \int \frac{d^3 \psi_i}{(2\pi)^3} e^{i \mathbf{\psi}_i \cdot \mathbf{r}_i} \prod_{i=1}^N \int \frac{d^3 \omega_i}{(2\pi)^3} e^{i \mathbf{\omega}_i \cdot \mathbf{r}_i} \prod_{i=1}^N \int \frac{d^3 \delta_i}{(2\pi)^3} e^{i \mathbf{\delta}_i \cdot \mathbf{r}_i} \prod_{i=1}^N \int \frac{d^3 \epsilon_i}{(2\pi)^3} e^{i \mathbf{\epsilon}_i \cdot \mathbf{r}_i} \prod_{i=1}^N \int \frac{d^3 \zeta_i}{(2\pi)^3} e^{i \mathbf{\zeta}_i \cdot \mathbf{r}_i} \prod_{i=1}^N \int \frac{d^3 \eta_i}{(2\pi)^3} e^{i \mathbf{\eta}_i \cdot \mathbf{r}_i} \prod_{i=1}^N \int \frac{d^3 \theta_i}{(2\pi)^3} e^{i \mathbf{\theta}_i \cdot \mathbf{r}_i} \prod_{i=1}^N \int \frac{d^3 \iota_i}{(2\pi)^3} e^{i \mathbf{\iota}_i \cdot \mathbf{r}_i} \prod_{i=1}^N \int \frac{d^3 \kappa_i}{(2\pi)^3} e^{i \mathbf{\kappa}_i \cdot \mathbf{r}_i} \prod_{i=1}^N \int \frac{d^3 \lambda_i}{(2\pi)^3} e^{i \mathbf{\lambda}_i \cdot \mathbf{r}_i} \prod_{i=1}^N \int \frac{d^3 \mu_i}{(2\pi)^3} e^{i \mathbf{\mu}_i \cdot \mathbf{r}_i} \prod_{i=1}^N \int \frac{d^3 \nu_i}{(2\pi)^3} e^{i \mathbf{\nu}_i \cdot \mathbf{r}_i} \prod_{i=1}^N \int \frac{d^3 \xi_i}{(2\pi)^3} e^{i \mathbf{\xi}_i \cdot \mathbf{r}_i} \prod_{i=1}^N \int \frac{d^3 \omicron_i}{(2\pi)^3} e^{i \mathbf{\omicron}_i \cdot \mathbf{r}_i} \prod_{i=1}^N \int \frac{d^3 \pi_i}{(2\pi)^3} e^{i \mathbf{\pi}_i \cdot \mathbf{r}_i} \prod_{i=1}^N \int \frac{d^3 \rho_i}{(2\pi)^3} e^{i \mathbf{\rho}_i \cdot \mathbf{r}_i} \prod_{i=1}^N \int \frac{d^3 \sigma_i}{(2\pi)^3} e^{i \mathbf{\sigma}_i \cdot \mathbf{r}_i} \prod_{i=1}^N \int \frac{d^3 \tau_i}{(2\pi)^3} e^{i \mathbf{\tau}_i \cdot \mathbf{r}_i} \prod_{i=1}^N \int \frac{d^3 \upsilon_i}{(2\pi)^3} e^{i \mathbf{\upsilon}_i \cdot \mathbf{r}_i} \prod_{i=1}^N \int \frac{d^3 \phi_i}{(2\pi)^3} e^{i \mathbf{\phi}_i \cdot \mathbf{r}_i} \prod_{i=1}^N \int \frac{d^3 \chi_i}{(2\pi)^3} e^{i \mathbf{\chi}_i \cdot \mathbf{r}_i} \prod_{i=1}^N \int \frac{d^3 \psi_i}{(2\pi)^3} e^{i \mathbf{\psi}_i \cdot \mathbf{r}_i} \prod_{i=1}^N \int \frac{d^3 \omega_i}{(2\pi)^3} e^{i \mathbf{\omega}_i \cdot \mathbf{r}_i} \prod_{i=1}^N \int \frac{d^3 \delta_i}{(2\pi)^3} e^{i \mathbf{\delta}_i \cdot \mathbf{r}_i} \prod_{i=1}^N \int \frac{d^3 \epsilon_i}{(2\pi)^3} e^{i \mathbf{\epsilon}_i \cdot \mathbf{r}_i} \prod_{i=1}^N \int \frac{d^3 \zeta_i}{(2\pi)^3} e^{i \mathbf{\zeta}_i \cdot \mathbf{r}_i} \prod_{i=1}^N \int \frac{d^3 \eta_i}{(2\pi)^3} e^{i \mathbf{\eta}_i \cdot \mathbf{r}_i} \prod_{i=1}^N \int \frac{d^3 \theta_i}{(2\pi)^3} e^{i \mathbf{\theta}_i \cdot \mathbf{r}_i} \prod_{i=1}^N \int \frac{d^3 \iota_i}{(2\pi)^3} e^{i \mathbf{\iota}_i \cdot \mathbf{r}_i} \prod_{i=1}^N \int \frac{d^3 \kappa_i}{(2\pi)^3} e^{i \mathbf{\kappa}_i \cdot \mathbf{r}_i} \prod_{i=1}^N \int \frac{d^3 \lambda_i}{(2\pi)^3} e^{i \mathbf{\lambda}_i \cdot \mathbf{r}_i} \prod_{i=1}^N \int \frac{d^3 \mu_i}{(2\pi)^3} e^{i \mathbf{\mu}_i \cdot \mathbf{r}_i} \prod_{i=1}^N \int \frac{d^3 \nu_i}{(2\pi)^3} e^{i \mathbf{\nu}_i \cdot \mathbf{r}_i} \prod_{i=1}^N \int \frac{d^3 \xi_i}{(2\pi)^3} e^{i \mathbf{\xi}_i \cdot \mathbf{r}_i} \prod_{i=1}^N \int \frac{d^3 \omicron_i}{(2\pi)^3} e^{i \mathbf{\omicron}_i \cdot \mathbf{r}_i} \prod_{i=1}^N \int \frac{d^3 \pi_i}{(2\pi)^3} e^{i \mathbf{\pi}_i \cdot \mathbf{r}_i} \prod_{i=1}^N \int \frac{d^3 \rho_i}{(2\pi)^3} e^{i \mathbf{\rho}_i \cdot \mathbf{r}_i} \prod_{i=1}^N \int \frac{d^3 \sigma_i}{(2\pi)^3} e^{i \mathbf{\sigma}_i \cdot \mathbf{r}_i} \prod_{i=1}^N \int \frac{d^3 \tau_i}{(2\pi)^3} e^{i \mathbf{\tau}_i \cdot \mathbf{r}_i} \prod_{i=1}^N \int \frac{d^3 \upsilon_i}{(2\pi)^3} e^{i \mathbf{\upsilon}_i \cdot \mathbf{r}_i} \prod_{i=1}^N \int \frac{d^3 \phi_i}{(2\pi)^3} e^{i \mathbf{\phi}_i \cdot \mathbf{r}_i} \prod_{i=1}^N \int \frac{d^3 \chi_i}{(2\pi)^3} e^{i \mathbf{\chi}_i \cdot \mathbf{r}_i} \prod_{i=1}^N \int \frac{d^3 \psi_i}{(2\pi)^3} e^{i \mathbf{\psi}_i \cdot \mathbf{r}_i} \prod_{i=1}^N \int \frac{d^3 \omega_i}{(2\pi)^3} e^{i \mathbf{\omega}_i \cdot \mathbf{r}_i} \prod_{i=1}^N \int \frac{d^3 \delta_i}{(2\pi)^3} e^{i \mathbf{\delta}_i \cdot \mathbf{r}_i} \prod_{i=1}^N \int \frac{d^3 \epsilon_i}{(2\pi)^3} e^{i \mathbf{\epsilon}_i \cdot \mathbf{r}_i} \prod_{i=1}^N \int \frac{d^3 \zeta_i}{(2\pi)^3} e^{i \mathbf{\zeta}_i \cdot \mathbf{r}_i} \prod_{i=1}^N \int \frac{d^3 \eta_i}{(2\pi)^3} e^{i \mathbf{\eta}_i \cdot \mathbf{r}_i} \prod_{i=1}^N \int \frac{d^3 \theta_i}{(2\pi)^3} e^{i \mathbf{\theta}_i \cdot \mathbf{r}_i} \prod_{i=1}^N \int \frac{d^3 \iota_i}{(2\pi)^3} e^{i \mathbf{\iota}_i \cdot \mathbf{r}_i} \prod_{i=1}^N \int \frac{d^3 \kappa_i}{(2\pi)^3} e^{i \mathbf{\kappa}_i \cdot \mathbf{r}_i} \prod_{i=1}^N \int \frac{d^3 \lambda_i}{(2\pi)^3} e^{i \mathbf{\lambda}_i \cdot \mathbf{r}_i} \prod_{i=1}^N \int \frac{d^3 \mu_i}{(2\pi)^3} e^{i \mathbf{\mu}_i \cdot \mathbf{r}_i} \prod_{i=1}^N \int \frac{d^3 \nu_i}{(2\pi)^3} e^{i \mathbf{\nu}_i \cdot \mathbf{r}_i} \prod_{i=1}^N \int \frac{d^3 \xi_i}{(2\pi)^3} e^{i \mathbf{\xi}_i \cdot \mathbf{r}_i} \prod_{i=1}^N \int \frac{d^3 \omicron_i}{(2\pi)^3} e^{i \mathbf{\omicron}_i \cdot \mathbf{r}_i} \prod_{i=1}^N \int \frac{d^3 \pi_i}{(2\pi)^3} e^{i \mathbf{\pi}_i \cdot \mathbf{r}_i} \prod_{i=1}^N \int \frac{d^3 \rho_i}{(2\pi)^3} e^{i \mathbf{\rho}_i \cdot \mathbf{r}_i} \prod_{i=1}^N \int \frac{d^3 \sigma_i}{(2\pi)^3} e^{i \mathbf{\sigma}_i \cdot \mathbf{r}_i} \prod_{i=1}^N \int \frac{d^3 \tau_i}{(2\pi)^3} e^{i \mathbf{\tau}_i \cdot \mathbf{r}_i} \prod_{i=1}^N \int \frac{d^3 \upsilon_i}{(2\pi)^3} e^{i \mathbf{\upsilon}_i \cdot \mathbf{r}_i} \prod_{i=1}^N \int \frac{d^3 \phi_i}{(2\pi)^3} e^{i \mathbf{\phi}_i \cdot \mathbf{r}_i} \prod_{i=1}^N \int \frac{d^3 \chi_i}{(2\pi)^3} e^{i \mathbf{\chi}_i \cdot \mathbf{r}_i} \prod_{i=1}^N \int \frac{d^3 \psi_i}{(2\pi)^3} e^{i \mathbf{\psi}_i \cdot \mathbf{r}_i} \prod_{i=1}^N \int \frac{d^3 \omega_i}{(2\pi)^3} e^{i \mathbf{\omega}_i \cdot \mathbf{r}_i} \prod_{i=1}^N \int \frac{d^3 \delta_i}{(2\pi)^3} e^{i \mathbf{\delta}_i \cdot \mathbf{r}_i} \prod_{i=1}^N \int \frac{d^3 \epsilon_i}{(2\pi)^3} e^{i \mathbf{\epsilon}_i \cdot \mathbf{r}_i} \prod_{i=1}^N \int \frac{d^3 \zeta_i}{(2\pi)^3} e^{i \mathbf{\zeta}_i \cdot \mathbf{r}_i} \prod_{i=1}^N \int \frac{d^3 \eta_i}{(2\pi)^3} e^{i \mathbf{\eta}_i \cdot \mathbf{r}_i} \prod_{i=1}^N \int \frac{d^3 \theta_i}{(2\pi)^3} e^{i \mathbf{\theta}_i \cdot \mathbf{r}_i} \prod_{i=1}^N \int \frac{d^3 \iota_i}{(2\pi)^3} e^{i \mathbf{\iota}_i \cdot \mathbf{r}_i} \prod_{i=1}^N \int \frac{d^3 \kappa_i}{(2\pi)^3} e^{i \mathbf{\kappa}_i \cdot \mathbf{r}_i} \prod_{i=1}^N \int \frac{d^3 \lambda_i}{(2\pi)^3} e^{i \mathbf{\lambda}_i \cdot \mathbf{r}_i} \prod_{i=1}^N \int \frac{d^3 \mu_i}{(2\pi)^3} e^{i \mathbf{\mu}_i \cdot \mathbf{r}_i} \prod_{i=1}^N \int \frac{d^3 \nu_i}{(2\pi)^3} e^{i \mathbf{\nu}_i \cdot \mathbf{r}_i} \prod_{i=1}^N \int \frac{d^3 \xi_i}{(2\pi)^3} e^{i \mathbf{\xi}_i \cdot \mathbf{r}_i} \prod_{i=1}^N \int \frac{d^3 \omicron_i}{(2\pi)^3} e^{i \mathbf{\omicron}_i \cdot \mathbf{r}_i} \prod_{i=1}^N \int \frac{d^3 \pi_i}{(2\pi)^3} e^{i \mathbf{\pi}_i \cdot \mathbf{r}_i} \prod_{i=1}^N \int \frac{d^3 \rho_i}{(2\pi)^3} e^{i \mathbf{\rho}_i \cdot \mathbf{r}_i} \prod_{i=1}^N \int \frac{d^3 \sigma_i}{(2\pi)^3} e^{i \mathbf{\sigma}_i \cdot \mathbf{r}_i} \prod_{i=1}^N \int \frac{d^3 \tau_i}{(2\pi)^3} e^{i \mathbf{\tau}_i \cdot \mathbf{r}_i} \prod_{i=1}^N \int \frac{d^3 \upsilon_i}{(2\pi)^3} e^{i \mathbf{\upsilon}_i \cdot \mathbf{r}_i} \prod_{i=1}^N \int \frac{d^3 \phi_i}{(2\pi)^3} e^{i \mathbf{\phi}_i \cdot \mathbf{r}_i} \prod_{i=1}^N \int \frac{d^3 \chi_i}{(2\pi)^3} e^{i \mathbf{\chi}_i \cdot \mathbf{r}_i} \prod_{i=1}^N \int \frac{d^3 \psi_i}{(2\pi)^3} e^{i \mathbf{\psi}_i \cdot \mathbf{r}_i} \prod_{i=1}^N \int \frac{d^3 \omega_i}{(2\pi)^3} e^{i \mathbf{\omega}_i \cdot \mathbf{r}_i} \prod_{i=1}^N \int \frac{d^3 \delta_i}{(2\pi)^3} e^{i \mathbf{\delta}_i \cdot \mathbf{r}_i} \prod_{i=1}^N \int \frac{d^3 \epsilon_i}{(2\pi)^3} e^{i \mathbf{\epsilon}_i \cdot \mathbf{r}_i} \prod_{i=1}^N \int \frac{d^3 \zeta_i}{(2\pi)^3} e^{i \mathbf{\zeta}_i \cdot \mathbf{r}_i} \prod_{i=1}^N \int \frac{d^3 \eta_i}{(2\pi)^3} e^{i \mathbf{\eta}_i \cdot \mathbf{r}_i} \prod_{i=1}^N \int \frac{d^3 \theta_i}{(2\pi)^3} e^{i \mathbf{\theta}_i \cdot \mathbf{r}_i} \prod_{i=1}^N \int \frac{d^3 \iota_i}{(2\pi)^3} e^{i \mathbf{\iota}_i \cdot \mathbf{r}_i} \prod_{i=1}^N \int \frac{d^3 \kappa_i}{(2\pi)^3} e^{i \mathbf{\kappa}_i \cdot \mathbf{r}_i} \prod_{i=1}^N \int \frac{d^3 \lambda_i}{(2\pi)^3} e^{i \mathbf{\lambda}_i \cdot \mathbf{r}_i} \prod_{i=1}^N \int \frac{d^3 \mu_i}{(2\pi)^3} e^{i \mathbf{\mu}_i \cdot \mathbf{r}_i} \prod_{i=1}^N \int \frac{d^3 \nu_i}{(2\pi)^3} e^{i \mathbf{\nu}_i \cdot \mathbf{r}_i} \prod_{i=1}^N \int \frac{d^3 \xi_i}{(2\pi)^3} e^{i \mathbf{\xi}_i \cdot \mathbf{r}_i} \prod_{i=1}^N \int \frac{d^3 \omicron_i}{(2\pi)^3} e^{i \mathbf{\omicron}_i \cdot \mathbf{r}_i} \prod_{i=1}^N \int \frac{d^3 \pi_i}{(2\pi)^3} e^{i \mathbf{\pi}_i \cdot \mathbf{r}_i} \prod_{i=1}^N \int \frac{d^3 \rho_i}{(2\pi)^3} e^{i \mathbf{\rho}_i \cdot \mathbf{r}_i} \prod_{i=1}^N \int \frac{d^3 \sigma_i}{(2\pi)^3} e^{i \mathbf{\sigma}_i \cdot \mathbf{r}_i} \prod_{i=1}^N \int \frac{d^3 \tau_i}{(2\pi)^3} e^{i \mathbf{\tau}_i \cdot \mathbf{r}_i} \prod_{i=1}^N \int \frac{d^3 \upsilon_i}{(2\pi)^3} e^{i \mathbf{\upsilon}_i \cdot \mathbf{r}_i} \prod_{i=1}^N \int \frac{d^3 \phi_i}{(2\pi)^3} e^{i \mathbf{\phi}_i \cdot \mathbf{r}_i} \prod_{i=1}^N \int \frac{d^3 \chi_i}{(2\pi)^3} e^{i \mathbf{\chi}_i \cdot \mathbf{r}_i} \prod_{i=1}^N \int \frac{d^3 \psi_i}{(2\pi)^3} e^{i \mathbf{\psi}_i \cdot \mathbf{r}_i} \prod_{i=1}^N \int \frac{d^3 \omega_i}{(2\pi)^3} e^{i \mathbf{\omega}_i \cdot \mathbf{r}_i} \prod_{i=1}^N \int \frac{d^3 \delta_i}{(2\pi)^3} e^{i \mathbf{\delta}_i \cdot \mathbf{r}_i} \prod_{i=1}^N \int \frac{d^3 \epsilon_i}{(2\pi)^3} e^{i \mathbf{\epsilon}_i \cdot \mathbf{r}_i} \prod_{i=1}^N \int \frac{d^3 \zeta_i}{(2\pi)^3} e^{i \mathbf{\zeta}_i \cdot \mathbf{r}_i} \prod_{i=1}^N \int \frac{d^3 \eta_i}{(2\pi)^3} e^{i \mathbf{\eta}_i \cdot \mathbf{r}_i} \prod_{i=1}^N \int \frac{d^3 \theta_i}{(2\pi)^3} e^{i \mathbf{\theta}_i \cdot \mathbf{r}_i} \prod_{i=1}^N \int \frac{d^3 \iota_i}{(2\pi)^3} e^{i \mathbf{\iota}_i \cdot \mathbf{r}_i} \prod_{i=1}^N \int \frac{d^3 \kappa_i}{(2\pi)^3} e^{i \mathbf{\kappa}_i \cdot \mathbf{r}_i} \prod_{i=1}^N \int \frac{d^3 \lambda_i}{(2\pi)^3} e^{i \mathbf{\lambda}_i \cdot \mathbf{r}_i} \prod_{i=1}^N \int \frac{d^3 \mu_i}{(2\pi)^3} e^{i \mathbf{\mu}_i \cdot \mathbf{r}_i} \prod_{i=1}^N \int \frac{d^3 \nu_i}{(2\pi)^3} e^{i \mathbf{\nu}_i \cdot \mathbf{r}_i} \prod_{i=1}^N \int \frac{d$$

from the delta-function slope-change requirements, that is, $k_{j+1} - k_j$ is determined by the boundary conditions at $z_i = z_j$. In the limit of a large sample, and defining $k_{j+1} - k_j = 1/L f(k_j)$, one can approximate $f(k_j)$ by a continuous function $f(k)$ which is the density of quasimomenta. The distribution of quasimomenta is then obtained as the solution to the following integral equation:

$$2 f(k) = 1 + \int_{-k_F}^{k_F} K(k-p) f(p) dp; \quad (2.6)$$

Here, the kernel function $K(k)$ is given by

$$K(k) = \frac{2c}{c^2 + k^2}; \quad (2.7)$$

and k_F is the maximum quasimomentum which determines the particle number density $n = N/L$ via

$$n = \int_{-k_F}^{k_F} f(k) dk \quad (2.8)$$

The corresponding ground-state energy is given by

$$E_0 = L \int_{-k_F}^{k_F} f(k) k^2 dk; \quad (2.9)$$

and is often written as $E_0 = N n^2 e()$, being an implicit function of n , via a dimensionless function $e()$ of the parameter $= c/n$.

Restoring the physical units, this gives an energy per particle:

$$E_0/N = \frac{\hbar^2}{2m} n^2 e(); \quad (2.10)$$

where

$$= \frac{m g}{\hbar^2 n}; \quad (2.11)$$

The dimensionless parameter which characterizes the strength of interactions is in fact the only parameter needed to describe the uniform 1D Bose gas at zero temperature. The limit of $= 1$ corresponds to the weakly interacting Gross-Pitaevskii (GP) regime, where the mean-field Bogoliubov theory works well. The opposite limit of $= 1$ corresponds to the strongly interacting or Tonks-Girardeau (TG) regime, and as $= 1$ one regains Girardeau's results for impenetrable bosons.

The solution to the ground state energy E_0 can be used, together with the Hellmann-Feynman theorem [23], for calculating an important observable { the normalized local pair correlation

$$g^{(2)}(0) = \frac{\langle \psi(z) \psi(z) \psi(z) \psi(z) \rangle}{n^2}; \quad (2.12)$$

The pair correlation is found by taking the derivative of the ground state energy with respect to the coupling constant g , owing to the fact that

$$\frac{dE_0}{dg} = \frac{d\hat{H}}{dg} = \frac{L}{2} \langle \psi(z) \psi(z) \psi(z) \psi(z) \rangle; \quad (2.13)$$

so that

$$g^{(2)}(0) = \frac{d e()} {d}; \quad (2.14)$$

The pair correlation $g^{(2)}(0)$ for the zero temperature uniform 1D Bose gas has been calculated using the Lieb-Liniger exact solution [7] for $e()$. The results are given in Ref. [15]. Here, we will extend these results (see Section III) to the case of a trapped (non-uniform) Bose gas using the local density approximation, and to finite temperatures as well.

C. Uniform gas at finite temperature

The excited states of the uniform 1D Bose gas can be calculated in a similar way, with each excited state corresponding to the removal of a quasimomentum with $|k| < k_F$ { called a hole } and the creation of a quasimomentum with $|k| > k_F$. In 1969, C.N. Yang and C.P. Yang [8] worked out the finite-temperature density matrix solution for the Lieb-Liniger model, by constructing the free energy and taking into account the entropy of all the different excited states. This was used in a subsequent work [9] to calculate numerically the pressure of the gas as a function of temperature.

At thermal equilibrium, we now assume that the density of quasimomenta $f(k)$ has no upper cut-off, and that it consists of two types of terms { occupied quasimomenta [with density $f_p(k)$] and unoccupied or 'hole' quasimomenta [with density $f_h(k)$], i.e. $f(k) = f_p(k) + f_h(k)$. The overall integral equation now has the form (using units in which $\hbar = 2m = 1$ and $c = m g = \hbar^2$)

$$2 f(k) = 2 \int_{-1}^1 [f_p(k) + f_h(k)] K(k-p) f_p(p) dp; \quad (2.15)$$

Hence, the particle density n is obtained from the occupied or particle quasimomenta

$$n = \int_{-1}^1 f_p(k) dk; \quad (2.16)$$

while the total energy is now

$$E_0 = L \int_{-1}^1 f_p(k) k^2 dk; \quad (2.17)$$

However, there is also an entropy involved, since there are many wavefunctions that are nearly the same, within a given range of values of $f_p(k)$ and $f_h(k)$. In fact, the number of choices compatible with a given dk value is

$$\frac{[f(k)L dk]!}{[f_p(k)L dk]! [f_h(k)L dk]!}; \quad (2.18)$$

Thus, the entropy is

$$S = L \int_{-1}^1 [f \ln f - f_p \ln f_p - f_h \ln f_h] dk; \quad (2.19)$$

Minimizing the total free energy $F = E - TS$ gives the thermal equilibrium distribution of holes and particles, where we choose temperature to be in energy units, so that $k_B = 1$. The minimization at a fixed average particle number requires the use of a Lagrange multiplier μ , and gives the result that the distribution $f_p(k)$ satisfies the integralequation

$$\frac{1}{2} f_p(k) \frac{1}{1 + e^{\mu(k)=T}} = 1 + \frac{1}{Z_1} \int_1^{\infty} K(k-p) f_p(p) dp; \quad (2.20)$$

where the excitation spectrum $\mu(k)$ is calculated from a second integralequation

$$\mu(k) = \frac{1}{2} \frac{1}{Z_1} \int_1^{\infty} K(k-p) \ln 1 + e^{\mu(p)=T} dp; \quad (2.21)$$

Here, μ can be shown to coincide with the chemical potential of the system, while the entropy and the free energy per particle are found from :

$$S/N = \frac{1}{n} \int_1^{\infty} f(k) \ln 1 + e^{\mu(k)=T} dk + \frac{1}{nT} \int_1^{\infty} f_p(k) \mu(k) dk; \quad (2.22)$$

$$F/N = \frac{1}{2n} \int_1^{\infty} \ln 1 + e^{\mu(k)=T} dk; \quad (2.23)$$

In addition, using the thermodynamic identity $F = PL + N\mu$, one can arrive at the following simple result for the pressure of the gas

$$P(\mu; T) = \frac{1}{2n} \int_1^{\infty} \ln 1 + e^{\mu(k)=T} dk; \quad (2.24)$$

To calculate the pair correlation $g^{(2)}(0)$ for a finite temperature gas one can again use the Hellmann-Feynman theorem [23]. Here, we consider the canonical partition function $Z = \exp(-F/T) = \text{Tr} \exp(-\hat{H}/T)$, where the trace is over the states of the system with a fixed particle number N , at temperature T . Taking the derivative of $F = -T \log Z$ with respect to the coupling constant g we obtain

$$\frac{\partial F}{\partial g} = \frac{1}{Z} \text{Tr} e^{-\hat{H}/T} \frac{\partial \hat{H}}{\partial g} = \frac{1}{2} \int_1^{\infty} \int_1^{\infty} V(z) V(z) V(z) V(z) dz; \quad (2.25)$$

Introducing the free energy per particle $f = F/N$ and restoring the physical units, this gives [16]:

$$g^{(2)}(0) = \frac{2}{Ln^2} \frac{\partial F}{\partial g} \bigg|_{N,T} = \frac{2m}{\hbar^2 n} \frac{\partial f(\mu; T)}{\partial \mu} \bigg|_{n,T}; \quad (2.26)$$

Here, $\mu = T/T_d$ is a dimensionless temperature parameter, with $T_d = \hbar^2 n^2 / 2m$ being the temperature of quantum degeneracy for a uniform gas. Hence, we have

$$= \frac{2m T}{\hbar^2 n^2}; \quad (2.27)$$

The pair of the dimensionless parameters μ and μ completely characterize the properties of a finite temperature uniform gas.

Alternatively, the local pair correlation $g^{(2)}(0)$ can be calculated within the grand canonical formalism. Here, we consider the grand canonical partition function $Z = \exp(-\Omega/T) = \text{Tr} \exp[(\hat{N} - \hat{H})/T]$, where $\Omega = F - \mu N = -PL$ is the grand canonical thermodynamic potential and P is the pressure. The trace is over the states of the system, at a fixed chemical potential and temperature T . Taking the derivative of $\Omega = -T \log Z$ with respect to the coupling g we obtain:

$$\begin{aligned} \frac{\partial \Omega}{\partial g} &= -T \frac{\partial \log Z}{\partial g} \\ &= \frac{1}{Z} \text{Tr} \frac{\partial (\hat{N} - \hat{H})}{\partial g} \exp[(\hat{N} - \hat{H})/T] \\ &= \frac{1}{2} \int_1^{\infty} \int_1^{\infty} V(z) V(z) V(z) V(z) dz; \end{aligned} \quad (2.28)$$

Thus, the normalized pair correlation $g^{(2)}(0)$ can be calculated using

$$g^{(2)}(0) = \frac{2}{Ln^2} \frac{\partial \Omega}{\partial g} \bigg|_{\mu,T} = \frac{1}{n^2} \frac{\partial P}{\partial g} \bigg|_{\mu,T}; \quad (2.29)$$

This requires the use of Eq. (2.24) for the pressure, which in turn is found after solving the Yang-Yang integralequations (2.20) and (2.21).

The local pair correlation for a finite temperature uniform gas has been first calculated in Ref. [16] using the exact solutions to the Yang-Yang integralequations (2.20) and (2.21), together with Eqs. (2.23) and (2.26). In Sections IV-V II, we will extend these results to the case of a trapped gas using the local density approximation.

D. Quasi-uniform approximation

In a quasi-uniform approximation, we suppose that the system can be divided into small regions of size z which is larger than a characteristic short-range correlation length l_c . In each of these regions we assume that the inhomogeneity of the gas is negligible so that it can be treated as a uniform gas.

In this case, the trapping potential $V(z)$ is replaced by a step-like function $V(z_j) = m \hbar^2 z_j^2 / 2$ which is constant within each region from z_j to z_{j+1} and undergoes step-like changes at the boundaries of the adjacent regions. Here, the size z takes the role of the length L from the Yang-Yang solution that applies to each region.

We now consider an ansatz in which the overall density matrix has the structure of an outer-product of canonical solutions, with N_j being the average number of particles in the j -th region:

$$\rho^N = \rho^{N_1}(z_1) \rho^{N_2}(z_2) \cdots \rho^{N_n}(z_n); \quad (2.30)$$

Next we look for an approximate solution in which the effective Hamiltonian is assumed to introduce no coupling between the regions. To obtain this we must now minimize the total free energy given by

$$F_N = \sum_{j=1}^{X^n} (E_j - T S_j); \quad (2.31)$$

This requires us to include a constraint on the total particle number:

$$N = \sum_{j=1}^{X^n} N_j; \quad (2.32)$$

Hence, it is appropriate to use a Lagrangian formulation with

$$L = \sum_{j=1}^{X^n} (E_j - T S_j - \mu_0 N_j); \quad (2.33)$$

We note here that the Lagrangian L is now simply a sum over independent regions, with each term corresponding to that for a single uniform Bose gas. As we are only constraining the total particle number, not the number in each region, the chemical potential is the same for each term. Since there is no explicit coupling between the regions, the Lagrangian is minimized when we satisfy the Yang-Yang equations in each separate region, but with the same (global) chemical potential μ_0 at all locations.

E. Local density approximation (LDA)

In more detail, we have shown that for a large system, where the density profile varies in a smooth way, the system behaves locally as a piece of a uniform gas. This can be described locally as a uniform gas with chemical potential equal to the local effective chemical potential

$$\mu(z) = \mu_0 - V(z) = \mu_0 - \frac{1}{2} m \omega_z^2 z^2; \quad (2.34)$$

where μ_0 is the global equilibrium chemical potential.

For the LDA to be valid, the short-range correlation length $\xi_c(z)$ should be much smaller than the characteristic inhomogeneity length $\xi_{inh}(z)$. These length scales depend on the displacement from the trap center z , and the LDA validity criterion reads:

$$\xi_c(z) \ll \xi_{inh}(z) = \frac{n(z)}{\left| \frac{dn(z)}{dz} \right|}; \quad (2.35)$$

The short-range correlation length $\xi_c(z)$ is defined locally via the density distribution $n(z)$. At low temperatures, the correlation length $\xi_c(z)$ can in general (irrespective of the interaction strength) be expressed via the local chemical potential $\mu(z)$:

$$\xi_c(z) = \frac{\hbar}{m \sqrt{2\mu(z)}}; \quad (T = T_0); \quad (2.36)$$

In the weakly interacting Gross-Pitaevskii (GP) regime the relation between the chemical potential $\mu(z)$ and the density $n(z)$ is $\mu(z) = g n(z)$, and we obtain that the correlation length coincides with the healing length $\xi_c(z) = \hbar / \sqrt{2 m g n(z)}$. In the strongly interacting Tonks-Girardeau (TG) regime one has $\mu(z) = \hbar^2 n^2(z) / (2m)$, so that $\xi_c(z) = 1/n(z)$, neglecting the numerical factor of order 1. At high temperatures, $\xi_c(z)$ is of the order of the thermal de Broglie wavelength λ_T .

The condition (2.35) is sufficient for using the LDA for calculating the density profiles and local correlation functions. The reason is that these correlations, in particular the two-particle correlation $g^{(2)}(0)$, are determined by the contribution of excitations which have energies of the order of the chemical potential and wavelength of the order of ξ_c . However, this is not the case for all correlation functions. For example, calculation of the finite-temperature single-particle correlation function would require a strong LDA condition in which the sample size was much larger than the phase correlation distance [27]. In this sense, one may call Eq. (2.35) the 'weak' LDA criterion. However, within the LDA, no correlation function can be calculated reliably over distance scales that are comparable to the sample size.

Thus, the 'weak' criterion of validity of the LDA requires that variations of the density occur on a length scale that is much larger than $\xi_c(z)$, in which case the gas is treated locally as a piece of a uniform gas. From the definition of $\xi_{inh}(z)$, one can easily see that the LDA is easier to satisfy in the center of the trap where the density profile is almost flat than near the tails of the distribution where the density drops rapidly. However, for measurements that average over an entire trap, it is the central region that plays the most important role.

III. ZERO-TEMPERATURE TRAPPED GAS

A. LDA criterion at $T = 0$

Here, we analyze the implications of the LDA criterion (2.35) for a zero temperature gas. At $T = 0$, a uniform 1D Bose gas can be characterized by a single dimensionless interaction parameter γ , Eq. (2.11). Depending on its value, one has two well-known and physically distinct regimes of quantum degeneracy. For $\gamma \gg 1$, i.e. at weak couplings or high densities, the gas is in a coherent or Gross-Pitaevskii (GP) regime. In this regime, long-range order is destroyed by long-wavelength phase

uctuations [24, 25, 26, 27] and the equilibrium state is a quasi-condensate characterized by suppressed density fluctuations. For strong couplings or low densities,

1, the gas reaches the strongly interacting or Tonks-Girardeau (TG) regime and undergoes "fermionization" [6, 7]. The term "fermionization" is used here in the sense that the wave function strongly decreases as particles approach each other.

For a trapped (non-uniform) gas one can introduce a local interaction parameter

$$g(z) = \frac{mg}{\sqrt{2}n(z)}; \quad (3.1)$$

which changes with the density distribution $n(z)$ and can be used for characterizing the local properties of the gas.

From the definition of $g(z)$ it is clear that as one moves from the center of the trap towards the tails of the density distribution where $n(z) \rightarrow 0$, the gas either enters the TG regime where $g(z) \rightarrow 1$, or else the LDA itself breaks down.

Moreover, in the $T = 0$ case the Lieb-Liniger solution within the LDA gives a density profile that vanishes [$n(z) = 0$] beyond a certain distance R from the origin [28, 29]. This distance is called the Thomas-Fermi radius and it is determined from the condition $R = \frac{1}{2} \sqrt{\frac{2m}{\mu}} = 0$ which gives:

$$R = \frac{2}{m} \sqrt{\frac{1}{2}}; \quad (3.2)$$

Since $n(z)$ vanishes exactly at $|z| = R$ [30], it is clear that the LDA criterion (2.35) can only be satisfied up to a certain maximum distance from the trap center $|z| = R$, displaced from R by $z(z = R)$. We would like therefore to determine the displacement z such that the LDA is valid for $0 \leq |z| \leq R - z$ and breaks down beyond $|z| = R - z$.

As we are interested in calculating the density profiles and the local two-particle correlation function, we will only focus on the weak LDA criterion, Eq. (2.35). First, we rewrite the inhomogeneity length scale from Eq. (2.35) in the following equivalent form

$$l_{inh}(z) = n(z) \frac{d g(z)}{d z} : \quad (3.3)$$

Using the explicit expression $g(z) = \frac{1}{\sqrt{2}n(z)}$ and taking its derivative, we obtain at $|z| = R - z(z = R)$:

$$l_{inh}(z) = \frac{n(z)}{m} \frac{d g(z)}{d z} : \quad (3.4)$$

Combining Eqs. (2.36) and (3.4), one can rewrite the LDA criterion $l_c(z) = l_{inh}(z)$ in the following equivalent form (again neglecting numerical factors of order one):

$$\frac{g(z)}{0} \frac{d \ln g(z)}{d \ln n(z)} = 1; \quad (3.5)$$

Next, we note that in the limiting GP and TG regimes the derivative $d \ln g(z) = d \ln n(z)$ is equal, respectively, to one and two, so in general $1 \leq d \ln g(z) \leq 2$. Therefore, the exact numerical value of this quantity can be replaced by unity in all regimes, and the LDA criterion becomes

$$\frac{g(z)}{0} \frac{d \ln g(z)}{d \ln n(z)} = 1; \quad (3.6)$$

Finally, expanding $g(z)$ near the edge of the cloud where $|z| = R - z(z = R)$, we obtain that $g(z) = \frac{1}{\sqrt{2}n(z)}$, so that the criterion of applicability of the LDA is reduced to a simple requirement:

$$\frac{z}{R} \frac{d \ln g(z)}{d \ln n(z)} = 1; \quad (3.7)$$

For $(0) = 1$, the local value of $g(z)$ at $|z| = R - z$ is

$$g(z) = \frac{mgR}{\sqrt{2}n(0)} = \frac{0}{\sqrt{2}n(z)}; \quad (3.8)$$

We see that if $(0) = (\sqrt{2}n(0))^{2/3}$ then $g(z) = 1$ at $|z| = R - z$, implying that the gas stays in the GP regime at all locations z until the LDA breaks down. If, on the other hand, $(0) = (\sqrt{2}n(0))^{2/3}$ then $g(z) = 1$ at $|z| = R - z$ so that the gas first approaches the TG regime and then the LDA breaks down.

For $(0) = 1$ the gas is in the TG regime at all locations z , until the LDA breaks down. This is because $g(z)$ is always larger than (0) , and hence $g(z) = 1$.

In the limiting cases of $(0) = 1$ and $(0) = 1$, the LDA criterion (3.7) can be conveniently rewritten in terms of (0) and the total number of particles N . In doing so we use the fact that the chemical potential is given by $\mu = gn(0)$ for $(0) = 1$, and by $\mu = \frac{1}{2} \sqrt{2} n^2(0) = (2m)$ for $(0) = 1$. In addition, we use the known relationship between the peak density $n(0)$ and N in each case [see Eqs. (3.14) and (3.18) below]. As a result, we obtain that the LDA criterion (3.7) can be rewritten as follows, in the GP and TG regimes, respectively:

$$\frac{z}{R} \frac{d \ln g(z)}{d \ln n(0)} = \frac{1}{(0)^{1/3} N^{2/3}}; \quad [(0) = 1]; \quad (3.9)$$

$$\frac{z}{R} \frac{d \ln g(z)}{d \ln n^2(0)} = \frac{1}{N^{2/3}}; \quad [(0) = 1]; \quad (3.10)$$

As we see, for any small but finite (0) in the GP regime, the right hand side of Eq. (3.9) can be made small by increasing the total number of particles N . For a fixed coupling g and a constant density $n(0)$ [such that (0) stays constant], the increase of the particle number N has to be accompanied by a reduction of the trap frequency ω_z . Thus, the ratio $z = R$ can also be made small, so that the LDA criterion in the GP regime $[(0) = 1]$ is satisfied for almost the entire sample, up

to the location $z = R$ z very close to the edge of the cloud. Similar considerations apply to the TG regime $[(0) \ll 1]$, where the requirement on the (large) total number of particles N is less stringent than in the GP regime.

B. Pair correlations at $T = 0$

Here we discuss the local pair correlation

$$g^{(2)}(z; z) = \frac{\langle \hat{\psi}^\dagger(z) \hat{\psi}^\dagger(z) \hat{\psi}(z) \hat{\psi}(z) \rangle}{n^2(z)} \quad (3.11)$$

in a zero temperature trapped gas within the LDA. The calculations are done using the solution to the Lieb-Liniger equation (2.6) and the Hellmann-Feynman theorem [23], Eq. (2.14). Here, $g^{(2)}(0)$ is now replaced by $g^{(2)}(z; z)$ and is to be understood as the local value of $g^{(2)}(z)$. Thus, to calculate $g^{(2)}(z; z)$ as a function of the distance from the trap centre, one can use the uniform results in which the interaction parameter $\gamma(z)$ is found from the density profile $n(z)$, for different values of (0) .

The implementation of the LDA, using the local effective chemical potential $\mu(z)$, Eq. (2.34), is carried out by means of first calculating the chemical potential as a function of n , and then inverting this dependence for obtaining $n(z)$. This gives $n(z)$ [and hence $\gamma(z)$] as a function of z , for a given value of the interaction parameter (0) at the trap center.

Depending on the value of the coordinate-dependent interaction parameter $\gamma(z)$, Eq. (3.1), we have the following limiting behavior of the pair correlation function.

In the Gross-Pitaevskii (GP) limit of a weakly interacting gas, the pair correlation in the uniform case is $g^{(2)} \approx 1 - \frac{1}{2} \gamma^2 = 1 - \frac{1}{2} \gamma^2$ [15]. For a trapped gas, replacing γ by $\gamma(z)$ gives:

$$g^{(2)}(z; z) \approx 1 - \frac{1}{2} \frac{\gamma^2(z)}{1 - \gamma^2(z)}; \quad \gamma(z) \ll 1: \quad (3.12)$$

where we have used the relationship between $\gamma(z)$ and $n(z)$ and the fact that in the GP regime the density profile is given by the familiar Thomas-Fermi parabola:

$$n(z) = n(0) (1 - z^2/R^2); \quad (3.13)$$

and $n(z) = 0$ for $|z| > R$. Here, the peak density $n(0)$ and the radius R are given by:

$$n(0) = \frac{9m N^2 \hbar^2}{32g}^{1/3}; \quad (3.14)$$

$$R = \frac{3N \hbar^2}{2m \hbar^2}^{1/3}; \quad (3.15)$$

In the Tonks-Girardeau (TG) limit of strong interactions, the uniform gas pair correlation is $g^{(2)} \approx 0$,

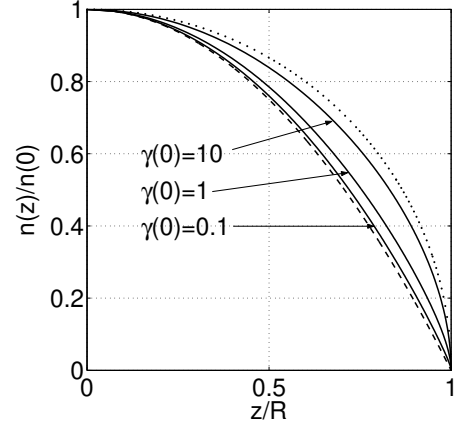


FIG. 1: Examples of the density profiles $n(z)/n(0)$ of a zero temperature 1D Bose gas in a harmonic trap as a function of the dimensionless coordinate z/R , for different values of the interaction parameter (0) . The solid lines are the results of the exact numerical solution of the Lieb-Liniger equations within the LDA. The dashed and the dotted lines are the analytic results given by the Thomas-Fermi parabola in the GP regime and the square root of parabola in the TG regime, respectively.

$4 - \gamma^2 = (3 - \gamma^2)^2$, [15]. In the trapped gas case, replacing γ by $\gamma(z)$ gives

$$g^{(2)}(z; z) \approx \frac{4 - \gamma^2(z) (1 - z^2/R^2)}{3 - \gamma^2(z)}; \quad \gamma(z) \ll 1; \quad (3.16)$$

where we again used the relationship between $\gamma(z)$ and $n(z)$ and the fact that the density profile in the TG regime is given by the square root of parabola:

$$n(z) = n(0) (1 - z^2/R^2)^{1/2}; \quad (3.17)$$

and $n(z) = 0$ for $|z| > R$. Here, the peak density $n(0)$ and the radius R are

$$n(0) = \frac{2m N \hbar^2}{2\pi}^{1/2}; \quad (3.18)$$

$$R = \frac{2\pi N \hbar^2}{m \hbar^2}^{1/2}; \quad (3.19)$$

In Fig. 1 we present the density profiles $n(z)$ as a function of the dimensionless coordinate z/R , for different values of (0) . The full lines represent the results of the numerical calculation within the LDA, which reproduce the results of Ref. [28], while the dashed and the dotted lines represent, respectively, the above analytic results in the GP and TG regimes.

Figure 2 shows the local pair correlation $g^{(2)}(z; z)$ as a function of z/R , for different values of (0) . As we see, for the case of weak interactions $(0) \ll 1$, the pair correlation is close to unity in the central bulk part of the distribution. This is an expected result for the coherent or GP regime. As one approaches the tails of the

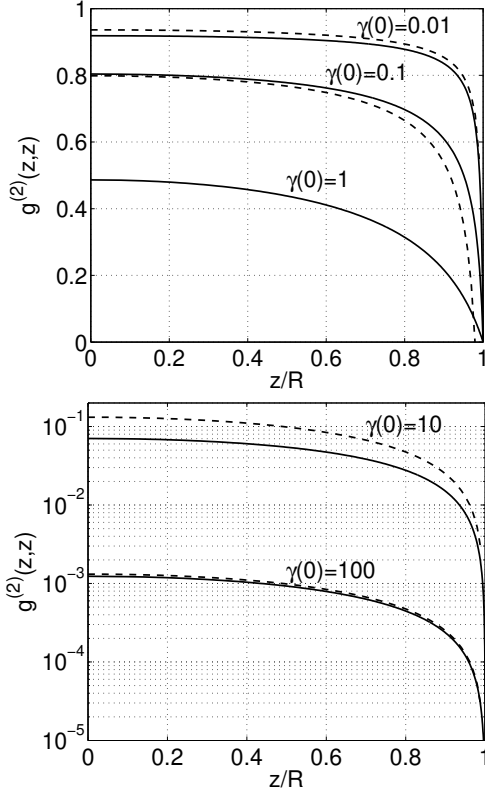


FIG. 2: The local pair correlation of a trapped 1D Bose gas at zero temperature, $g^{(2)}(z; z)$, as a function of the displacement from the trap center z/R , for different values of $\gamma(0)$. The full lines are the results of numerical calculation, while the dashed lines for $\gamma(0) = 0.01; 0.1$ and $\gamma(0) = 10; 100$ are the respective analytic results of Eqs. (3.12) and (3.16) shown for comparison.

distribution, where the density is reduced and $\gamma(z)$ becomes larger than one, the gas locally approaches the TG regime of 'Fermionization'. Here, the pair correlation is suppressed below the coherent level, $g^{(2)}(z; z) < 1$.

For the cases where $\gamma(0) \ll 1$, including the TG regime of $\gamma(0) \approx 1$, the pair correlation is suppressed across the entire sample. In the limit $\gamma(0) \gg 1$, the gas acquires pronounced 'fermionic' properties so that the wave function strongly decreases as particles approach each other, thus resulting in $g^{(2)}(z; z) \rightarrow 0$.

IV. FINITE TEMPERATURE TRAPPED GAS

A. Key parameters

An obvious choice of dimensionless interaction and temperature parameters for describing a trapped 1D Bose gas within the LDA consists in using the local value of the interaction parameter $\gamma(0)$ and the reduced temperature $t(0)$ in the trap center.

These are the same parameters that are used in the uni-

form gas treatment [16], Eqs. (2.11) and (2.27), except that now we define them via the local density $n(z)$. Thus, in general, we define the local interaction parameter $\gamma(z)$ and the local reduced temperature $t(z)$, according to:

$$\gamma(z) = \frac{m g}{\hbar^2 n(z)}; \quad (4.1)$$

$$t(z) = \frac{T}{T_d(z)} = \frac{2m T}{\hbar^2 n^2(z)}; \quad (4.2)$$

where $T_d(z) = \hbar^2 n^2(z)/(2m)$ is the local temperature of quantum degeneracy that corresponds (locally) to the conditions where the mean inter-particle separation becomes of the order of the thermal de Broglie wavelength.

The values of these parameters at the trap center, $\gamma(0)$ and $t(0)$, completely characterize all relevant properties of the gas within the LDA, including the associated density profiles $n(z)$, the resulting total number of particles N , as well as the correlation functions and the thermodynamic properties.

A completely equivalent pair of the interaction and temperature parameters, which is, however, more suitable for practical purposes is the local value of $\gamma(z)$ and a new temperature parameter t defined via:

$$t = \frac{\gamma(0)}{\gamma^2(0)} = \frac{\gamma(z)}{\gamma^2(z)} = \frac{T}{m g^2/(2\hbar^2)}; \quad (4.3)$$

According to this definition, the temperature is measured in units of the characteristic energy $E_b = m g^2/(2\hbar^2)$.

The advantage of using t as the dimensionless temperature parameter is that it is independent of the density and gives a direct measure of the global temperature of the gas, which in equilibrium is the same for the entire sample. This allows us to easily explore the 'interaction { temperature' parameter space $[\gamma(0) - t]$ in a systematic way. For example, considering different values of $\gamma(0)$ while t is kept constant would correspond to physical conditions under which the peak density of the gas $n(0)$ is varied while the absolute temperature T is kept unchanged. A novel experimental technique that implemented this approach for achieving a Bose-Einstein condensation in a 3D gas has recently been demonstrated in Ref. [31].

Other alternative choices are possible for characterizing the interactions and temperature of a trapped gas in dimensionless units. For example, to characterize the system at different temperatures T while the total number of particles N is kept constant, one can define an alternative pair of global parameters which are more suitable for this case (see Sec. V I). Here, the global temperature parameter can be defined as $\tau = T/T_Q$, where $T_Q = N^{-1/z}$ is the global temperature of quantum degeneracy of a trapped gas (in energy units, $k_B = 1$, where k_B is the Boltzmann constant). Irrespective of the interaction strength, a harmonically trapped Bose gas at $T = T_Q$ obeys the classical Boltzmann statistics, whereas for $T < T_Q$ quantum statistical effects become important. This is clearly seen in the limit of a trapped ideal gas ($\gamma(0) \rightarrow 0$) and in the

opposite limit of a strongly interacting gas ($\rho \rightarrow 1$). In the latter case, the problem maps onto the trapped gas of non-interacting fermions [6]. So, in both limits T_Q appears explicitly as the temperature of quantum degeneracy for the trapped sample as a whole.

B. LDA criterion at finite T

Here we analyze the local density approximation for a finite temperature gas, and obtain simple criteria for its validity in the limiting cases of very high and very low temperatures, $T \gg T_Q$ and $T \ll T_Q$.

In the high temperature limit, $T \gg T_Q$ [in which case $\rho \ll 1$ ($T=T_Q$)²], the density distribution $n(z)$ can be approximated by a Gaussian profile in all regimes, as the interaction between the particles is negligible compared to their thermal kinetic energies. For N particles at temperature T in a harmonic trap of frequency ω_z , the density profile is determined by the thermal distribution for a classical ideal gas described by Boltzmann statistics:

$$n_T(z) = \frac{N}{R_T} \exp(-z^2/R_T^2); \quad (4.4)$$

where the radius R_T characterizes the width of the Gaussian and is given by

$$R_T = \sqrt{\frac{2T}{m\omega_z^2}}; \quad (4.5)$$

In this high-temperature limit, the correlation length is given by the thermal de Broglie wavelength λ_T , so that the LDA criterion (2.35) gives:

$$z \ll \frac{T}{\omega_z} \sqrt{\frac{2T}{m\omega_z^2}} = \frac{T}{\omega_z} R_T; \quad (T \gg T_Q): \quad (4.6)$$

Since $T \gg T_Q = N \omega_z$ implies that $T \gg \omega_z$, the above LDA criterion can be satisfied for all locations z from the trap center up to distances equal to several characteristic widths R_T . For sufficiently large total number of particles N , the ratio $T \gg \omega_z$ will be even larger so that the LDA will be valid for even larger distance from the trap center.

In the opposite limit of low temperatures $T \ll T_Q$ [in which case $\rho \gg 1$ ($T=T_Q$)² for $\rho \ll 1$, and $\rho \gg 1$ ($T=T_Q$)² for $\rho \gg 1$], the density profile $n(z)$ can be approximated by two contributions. The first one is for the central bulk part which will be close to the $T = 0$ density profile up to a certain distance $|z| \ll R$ ($z \ll R$) from the trap center. Here R is the zero-temperature Thomas-Fermi radius, Eq. (3.2). The second contribution is for the tails of the distribution which can be approximated by a thermal Gaussian.

As before, we will focus on the 'weak' LDA condition (2.35) involving the correlation length $l_c(z)$. For the central part of the sample, up to distances $|z| \ll R$ ($z \ll R$), we can use the LDA criterion derived for the zero temperature gas, Eq. (3.7). In the weakly and strongly interacting limits this can be rewritten (as before) in terms of the interaction parameter ρ and the total number of particles N [see Eqs. (3.9) and (3.10)].

For the Gaussian tails of the distribution, i.e. at distances $|z| \gg R$, where the local correlation length is given by λ_T , we use the above high-temperature result, Eq. (4.6), and rewrite it in terms of the Thomas-Fermi radius R and the global chemical potential μ_0 . As a result, the LDA criterion for the Gaussian tails of a low-temperature gas can be written in the following form:

$$z \ll \frac{T}{\omega_z} \sqrt{\frac{2T}{m\omega_z^2}} = \frac{\mu_0}{\omega_z} R; \quad (T \gg T_Q): \quad (4.7)$$

In the GP regime [$\rho \ll 1$], where $\mu_0 \approx \ln(\rho)$, this gives:

$$z \ll R \rho^{1/2} N; \quad (4.8)$$

Thus, in order that the LDA works in the tails of the density distribution ($|z| \gg R$) in the GP regime, one has to have $\rho^{1/2} N \gg 1$. This requirement can always be satisfied with a sufficiently large number of particles N . For example, for $\rho = 3.8 \times 10^{-3}$ [which can be obtained, for example, with $\rho = 0.01$ and $T=T_Q = 0.01$, according to the relationship $\rho \approx 8 \sqrt{2} (0)T = (3T_Q)$ valid in this regime] one would need to have $N \approx 870$ in order to satisfy the LDA criterion for distances $R \ll z \ll 20R$.

In the TG regime [$\rho \gg 1$], where $\mu_0 \approx 2 \ln(\rho)$, Eq. (4.7) again reduces to the condition given by Eq. (4.8). Thus, in the TG regime the validity of the LDA in the tails of the distribution again requires that $\rho^{1/2} N \gg 1$. However, now we have $\rho \approx 2T/T_Q$, for $T \gg T_Q$.

To summarize, in the low temperature limit the LDA criterion can be easily satisfied for the central bulk part of the density distribution and for the Gaussian tails. This leaves the question of validity of the LDA in the low-density region near $z = R$, where the density may vary more rapidly.

We note, however, that at small finite temperatures the variation of the density profile around $z = R$ is more smooth than in the $T = 0$ limit, so that the LDA criterion may still be satisfied in this region, in contrast to the $T = 0$ case where the LDA necessarily breaks down as one approaches the edge of the cloud at $z = R$. More importantly, the LDA becomes valid again for distances past the small critical region around $z = R$, i.e. in the tails of the density distribution. This means that the results of calculation of the pair correlation function $g^{(2)}(z; z)$ at small finite temperatures should be valid everywhere except in a small region around $z = R$. At high temperatures the LDA criterion becomes less restrictive, and can be satisfied for the entire sample.

C. Calculating the local pair correlation and density profiles

The local pair correlation $g^{(2)}(z; z)$, Eq. (3.11), as a function of the location z from the trap center is calculated using Eq. (2.29) in which is replaced by the local chemical potential $\mu(z) = \mu_0 - V(z)$ and where n is the local density $n(z)$. The calculation is based on iterative numerical solution of the Yang-Yang exact integral equations [8] for the excitation spectrum and for the distribution function of "quasimomenta", (2.20) and (2.21). For a given set of values of μ_0 , T and g , this gives the resulting density profile $n(z)$, Eq. (2.16), and the pressure P , Eq. (2.24). Differentiating P with respect to g gives the local pair correlation $g^{(2)}(z; z)$.

A convenient way to implement the numerical algorithm for solving the Yang-Yang equations is via a dimensionless coordinate

$$\xi = \frac{z}{R_T}; \quad (4.9)$$

where the length scale R_T is the thermal width of the classical Gaussian distribution $n_T(z)$, given by Eq. (4.5).

Using the dimensionless coordinate ξ , the local chemical potential can be rewritten as

$$(\mu_T) = \mu_0 - T^2; \quad (4.10)$$

After setting up a lattice of ξ values, $f_{\xi}g$, the solution to the Yang-Yang equations proceeds as in the case of a uniform gas, with the input parameters being an array of the values of the local chemical potential $\mu_i = (\mu_T)_i$, the temperature T , and the coupling parameter g , as described above.

The numerical results are then presented in terms of the dimensionless parameters μ_0 and the temperature parameter $t = T_0/T$ (or t), where we note that

$$\frac{n(z)}{n(0)} = \frac{(\mu_0)}{(\mu_T)}; \quad (4.11)$$

This makes the output results scalable with respect to the physical parameters, rather than dependent of their absolute values.

The total number of particles in the system is calculated from the resulting density profile $n(z)$ via

$$N = \int_{-Z}^Z n(z) dz; \quad (4.12)$$

Using the dimensionless coordinate ξ and Eq. (4.11) this can be rewritten as

$$N = \frac{R_T m g}{\sim^2} \frac{1}{n(0)} \int_{-1}^{1} \frac{(\mu_0)}{(\mu_T)} d\xi; \quad (4.13)$$

so that the dimensionless ratio T_0/T is given by

$$\frac{T_0}{T} = \frac{2}{\mu_0} \int_{-1}^{1} \frac{d\xi}{(\mu_T)}; \quad (4.14)$$

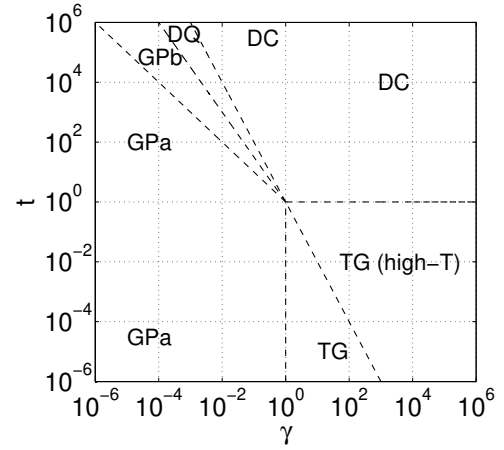


FIG. 3: Diagram of different regimes of a uniform 1D Bose gas in the $(\mu_0 - t)$ plane. The labels TG, GP, DQ and DC refer to the Tonks-Girardeau, Gross-Pitaevskii, decoherent quantum and decoherent classical regimes, respectively. Although all transitions are continuous, for purposes of discussion we classify the distinct regimes as follows:

TG: $t > 1, t < 2$; TG (high-T): $2 < t < 1$;
 GPa: $t < 1, t < 1$; GPb: $1 < t < 3=2$;
 DQ: $3=2 < t < 2$; DC: $t > \max f1; 2g$.

This gives a relationship between the global and local dimensionless parameters and allows us to present the numerical results in a scalable fashion, rather than in terms of the absolute values of N , T , μ_0 , and g . Here, the desired values of T_0/T can be achieved by varying the ratio μ_0/T of the input parameters μ_0 and T .

V. DENSITY PROFILES AND PAIR CORRELATIONS

A. Regimes in a uniform gas

In order to understand the results for the pair correlations $g^{(2)}(z; z)$ of a trapped 1D Bose gas, we first recall the classification of the regimes of a uniform gas. In Ref. [16], these were identified using the results for the local pair correlation $g^{(2)}$ in terms of the interaction parameter and the reduced temperature t . Here, we give a brief summary of these results, except that we rewrite them in terms of the parameters μ_0 and $t = T_0/T$, instead of μ_0 and T . This is completely equivalent to the original pair. The new parameters μ_0 and t are more suitable for exploring the properties of the trapped gases, as discussed in Sec. IV A.

The diagram representing these different regimes for a uniform 1D Bose gas in the parameter space $(\mu_0 - t)$ is shown in Fig. 3. The regimes are classified as follows:

Strong coupling regime: In the strong coupling TG regime of 'Fermi ionization', where $t > 1$ and the temperature $T < T_d$ ($t < 1$ or $t < 2$), we only have a small correction compared to the zero temperature result

[16, 32]:

$$g^{(2)} \sim \frac{4}{3} - \frac{1}{2} + \frac{4t^2}{4^2}; \quad t \ll 1; \quad \text{TG:} \quad (5.1)$$

In the case of strongly interacting nondegenerate bosons, where $\mu = 0$ and the temperature $T = T_d$ ($1 \ll t^2$ or $t^2 \ll 1$), we have the regime of high-temperature 'fermionization'. Despite the temperature $T = T_d$, the local pair correlation is strongly suppressed ($g^{(2)} \ll 1$) [16, 32]:

$$g^{(2)} \sim 2t; \quad t \ll 1; \quad \text{TG (high-T):} \quad (5.2)$$

Gross-Pitaevskii regime: In the GP regime, where $\mu = \mu_0$ and at temperatures $T = 2T_d$ (or $t \ll 1$) the finite temperature correction to the zero temperature result is again very small [16]:

$$g^{(2)} \sim 1 - \frac{2\mu_0}{24} t^2 \ll 1; \quad t \ll 1; \quad \text{GPa:} \quad (5.3)$$

For $T = 2T_d$ (or $t \ll 1$), the finite temperature correction is the leading one. It is important to recognize that the upper bound for the GP regime extends only up to temperatures of the order of $T = T_d$ (or $t \ll 1$), and not to $T = T_d$. Here, the temperature T_d is responsible for the presence of the quantum degeneracy, while T_d for the presence of phase coherence. Thus, for $T = T_d$, the finite temperature GP regime lies within the temperature interval $2T_d \gg T \gg T_d$ (or $1 \ll t \ll 3$), and the pair correlation here is given by [16]:

$$g^{(2)} \sim 1 + \frac{1}{2} t^2; \quad 1 \ll t \ll 3; \quad \text{GPb:} \quad (5.4)$$

Decoherent regime: $t \gg \max(1, 3)$. Due to the existence of two characteristic temperatures in the 1D uniform gas, T_d and T_d , at temperatures T higher than T_d one has two sub-regions. For temperatures in the interval $T_d \ll T \ll T_d$ ($1 \ll t \ll 3$ or $t^2 \ll 1$) the gas is in the decoherent quantum (DQ) regime, while for $T \gg T_d$ ($t \ll 1$ or $t^2 \ll 1$) the gas is in the decoherent classical (DC) regime. In both cases the local pair correlation is close to $g^{(2)} \sim 2$ [16]:

$$g^{(2)} \sim 2 - 4t^2; \quad t \ll 1; \quad \text{DQ;} \quad (5.5)$$

$$g^{(2)} \sim 2 - \frac{2}{t}; \quad t \gg 1; \quad \text{DC:} \quad (5.6)$$

The result in the DC regime remains valid for large t , provided $t^2 \ll 1$ (or $t^2 \ll 1$) [16], and we can combine the required conditions on temperature via $\max(t^2, 1)$.

B. Regimes in a trapped gas

In a harmonically trapped finite-temperature 1D Bose gas we again have a strong coupling regime, weak coupling GP regime, and a decoherent regime. The results for the local pair correlation $g^{(2)}(z; z)$ in the first two regimes are easily obtained from Eqs. (5.1)–(5.4) by replacing the interaction parameter by the local z -dependent value $\mu(z)$ of the trapped sample. However, it is convenient to rewrite the results for the local correlation $g^{(2)}(0; 0)$ in the trap center in terms of $\mu(0)$ and the temperature parameter $T = T_0$, where $T_0 = N^{-1} \mu(0)$ is the global temperature of quantum degeneracy of the sample as a whole.

Strong coupling regime. In the strong coupling TG regime, where $\mu(0) \ll 1$ and $T = T_0$, the density profile is given by the Thomas-Fermi result, Eq. (3.17), and this allows one to establish the relationship between the temperature parameters t and μ , using $\mu(0) = \mu(0) = T = T_0$ valid in this regime. Thus, $t^2 = \mu(0)$ and Eq. (5.1) transforms into:

$$g^{(2)}(0; 0) \sim \frac{4}{3} \mu(0) + \frac{1}{4} \mu(0)^2; \quad (5.7)$$

where $1 \ll \mu(0) \ll 1$.

For the regime of high-temperature fermionization at $T = T_0$, the density profile is given by the thermal Gaussian, Eq. (4.4), so that $\mu(0) = 4(T = T_0)^2$ and hence $t^2 = 4\mu(0)$. Therefore, Eq. (5.2) transforms into:

$$g^{(2)}(0; 0) = \frac{8}{2} \mu(0); \quad (5.8)$$

where $1 \ll \mu(0) \ll 1$.

Gross-Pitaevskii regime. In the GP regime ($\mu(0) \gg 1$), for temperatures $T = T_0$, the density profile is given by the Thomas-Fermi inverted parabola, Eq. (3.13). We then have $\mu(0) = 8(T = T_0)^2$ or $t^2 = 8\mu(0)$ [16], so that Eq. (5.3) transforms into

$$g^{(2)}(0; 0) = 1 - \frac{2\mu_0}{27} \mu(0) + \frac{16}{27} \mu(0)^2; \quad (5.9)$$

where $3 \ll \mu(0) \ll 1$ ($0.27 \ll \mu(0) \ll 1$) and $\mu(0) \gg 1$. Similarly, Eq. (5.4) transforms into

$$g^{(2)}(0; 0) = 1 + \frac{4}{3} \mu(0); \quad (5.10)$$

where $3 \ll \mu(0) \ll 1$ ($0.27 \ll \mu(0) \ll 1$) and $\mu(0) \gg 1$.

It is important to emphasize that for small $\mu(0)$ and making the temperature sufficiently low ($T = T_0 = 1$) the gas is always in the Gross-Pitaevskii regime.

Decoherent regime. For $T = T_0$, a harmonically trapped 1D Bose gas is in the decoherent classical regime. Here, the density profile is given by the thermal Gaussian, Eq. (4.4), so that $\mu(0) = 4(T = T_0)^2$ and hence

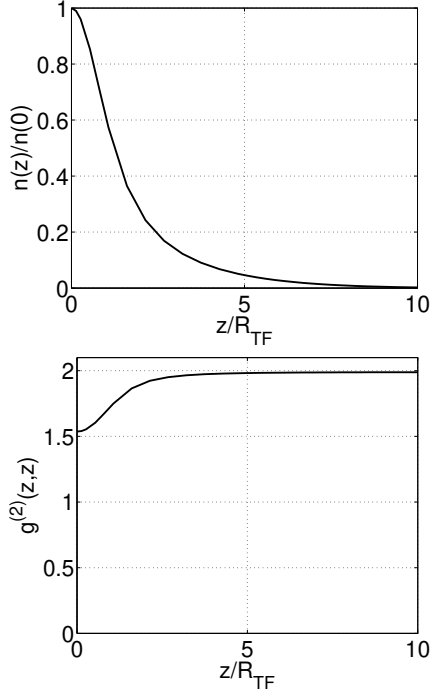


FIG. 4: Density profile $n(z)/n(0)$ and the local pair correlation $g^{(2)}(z;z)$ as a function of the distance from the trap center $z=R_{TF}$, for $T = 0.2T_Q$ ($t = 5 \cdot 10^4$) and $\rho(0) = 1.14 \cdot 10^3$. This corresponds to case 1b in the diagram of Fig. 6 below.

$t \ll 1$ $g^{(2)} = 2 \frac{\rho(0)}{\rho^2}$. Accordingly, Eq. (5.6) transforms into:

$$g^{(2)} = 2 \frac{\rho(0)}{\rho^2}; \quad (5.11)$$

where ρ is maximal; $\rho(0)g$, neglecting a numerical factor of the order of one. Thus, the validity of this result requires $\rho \gg 1$ for $\rho(0) < 1$, and $\rho(0) \gg 1$ for $\rho(0) > 1$.

In the case of small $\rho(0)$ and at temperatures $T \ll T_Q$, one has a crossover from the classical decoherent ($T \gg T_Q$) regime to the GP ($T \ll T_Q$) regime. The properties of the gas in this region can be treated as containing (locally) features of the decoherent quantum regime of the uniform gas. An example illustrating this behaviour is given in Fig. 4 where we plot the density profile $n(z)$ and the local pair correlation $g^{(2)}(z;z)$ as a function of z/R_{TF} where R_{TF} is the Thomas-Fermi radius in the GP regime. These are calculated numerically using the solution to the Yang-Yang integral equations, with a value of $\rho(0) = 1.14 \cdot 10^3$ at the trap center.

The temperature in this example is $T = 0.2T_Q$, which is intermediate between the decoherent classical and the GP regimes. Locally, the tails of the density profile are in the decoherent classical regime. On the other hand, the central part has features of the decoherent quantum regime. The curve for $g^{(2)}(z;z)$ shows that fluctuations well above the coherent level, with $g^{(2)}(0;0) \approx 1.5$, can occur even at temperatures below the transition to a quantum gas. However, with further temperature reduc-

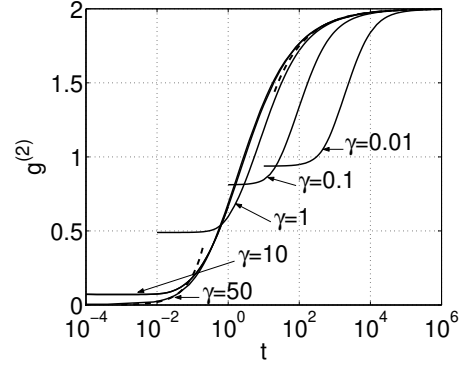


FIG. 5: Local pair correlation $g^{(2)}$ as a function of the reduced temperature t , for different values of the interaction parameter γ . The solid lines are the exact numerical results, while the dashed lines correspond to the approximate analytic result of Eq. (5.12).

tion well below T_Q , the density profile shrinks and one always has a coherent GP regime. For smaller values of γ , the temperature at which the coherent regime emerges must in general be calculated numerically.

C. Variation with temperature

In Fig. 5, we illustrate different regimes by plotting the local pair correlation $g^{(2)}$ as a function of the temperature parameter t , for different values of γ .

For sufficiently large γ the pair correlation approaches a universal function of the parameter t :

$$\lim_{t \rightarrow 1} g^{(2)} = \frac{2t}{2-t}; \quad t \ll 1; \quad (5.12)$$

This is because by increasing γ one can always reach locally the condition $t \ll 1$. Then, for $t \ll 1$ one has (locally) the regime of high-temperature fermionization and can use Eq. (5.2), whereas for $t \gg 1$ the sample will be in the decoherent classical regime described by Eq. (5.6).

This has an interesting consequence at sufficiently low temperatures $t \ll 1$. For $\gamma \gg 1$, which is always the case for far tails of the density distribution, the pair correlation remains suppressed below the coherent level ($g^{(2)} < 1$) rather than approaches the value of $g^{(2)} \approx 2$. This occurs despite the gas is locally not quantum degenerate at low density. One thus sees that fermionization in which the Bose gas develops antibunching with $g^{(2)} \rightarrow 0$ is an explicitly low-temperature phenomenon, when the temperature is scaled relative to the interaction strength.

However, for $\gamma \ll 1$ the suppression of pair correlations is not temperature-independent. Instead, the numerical results for increasing γ converge to a single universal function of t .

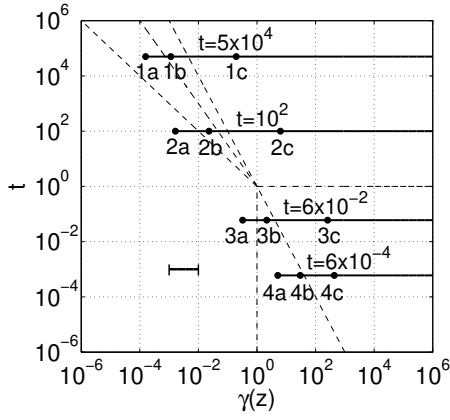


FIG. 6: Same as in Fig. 3, except with four horizontal lines at different temperatures t . This explores different density profiles in the parameter space $[(0)-t]$, where the points 1a-1c, 2a-2c, 3a-3c, and 4a-4c (marked by circles) are representative examples corresponding to different values of (0) at the trap center, at different temperatures t .

D. Spatial variation

In the case of a trapped gas, the same diagram of Fig. 3 also describes the spatial variation of the gas within the LDA. The parameter now becomes position dependent, (z) , due to the dependence on the density $n(z)$. In this diagram, any point on the $(-t)$ plane can be thought of as representing the interaction parameter (0) evaluated at the trap center, and the dimensionless temperature t . This is sufficient to completely characterize the properties of the trapped gas. The subsequent local values of (z) of such a gas (as one moves from the trap center towards the tails of the density distribution) can be represented by a horizontal line drawn in the direction of increasing (z) at constant t .

This is shown in Fig. 6, where the four horizontal lines correspond to four different temperatures t , while various points along each line represent different 'initial' values of the interaction parameter (0) . The interval in the left lower corner of the diagram shows the displacement (notice the logarithmic scale) for which the local value of (z) is increased by a factor of 10. This corresponds to a 10 fold decrease in the density $n(z)$. For any given distribution with the value of (0) in the center, this interval helps to immediately determine what fraction of the density profile relative to the peak density $n(0)$ is contained within a certain regime.

In the very far tails ($z \gg 1$) of any density distribution, where $n(z)$ vanishes and $(z) \gg 1$, we always enter either the DC or the high-temperature TG regime, depending on the temperature t . In addition, by considering a sample at any fixed temperature t , while the peak density is increased [(0) is decreased], one can always reach the situation where the bulk of the density distribution is in the GP regime where $g^{(2)}(z; z) \approx 1$. Physically, this can be achieved by adding more particles

to the system while maintaining the same global temperature T , under constant coupling g . From Fig. 5 it is clear that the density required may be relatively high, with $(0) = 0.01$ being necessary to have a limiting value of $g^{(2)} \approx 0.9$ at $t = 10^2$, as an example. For $(0) > 1$, there is no coherent GP regime over the entire range of temperatures.

To illustrate different examples, we now calculate the density profiles $n(z) = n(0)$ and the local pair correlations $g^{(2)}(z; z)$ as a function of the distance from the trap center z . The distance z is conveniently plotted in units of the Thomas-Fermi radius in the GP regime, R_{TF} , given by by Eq. (3.15). The relationship between $z = R_{TF}$ and the dimensionless coordinate $\bar{z} = z/R_T$ is: $z = R_{TF} = (\bar{z}^2/4)^{1/3} t^{1/2} (0)^{1/2}$. For a gas with a given coupling constant g , the temperature parameter t gives the measure of the absolute temperature T . In this sense, the examples with $t > 1$ and $t < 1$ in Fig. 6 represent high- and low-temperature limits, which we analyze separately.

1. High-temperature case

In Fig. 7 we present examples of calculated density profiles $n(z)$ and local pair correlations $g^{(2)}(z; z)$, for the high-temperature cases of $t = 5 \times 10^4$ and $t = 10^2$. The examples shown correspond to the points marked by circles 1a-1c and 2a-2c in the diagram of Fig. 6. For each temperature t , the sequence of points 1a, 1b and 1c (and similarly for 2a, 2b and 2c) corresponds to a decreasing peak density of the gas [increasing values of (0)], while the absolute temperature T is kept constant. This can be achieved by decreasing the total number of particles N in the sample, at constant T .

The examples 1c and 2c represent a low-density (non-degenerate) gas in the decoherent classical (DC) regime. The corresponding density profiles are well approximated by a thermal Gaussian, Eq. (4.4), and are omitted from the graphs for clarity. The respective second-order correlation functions $g^{(2)}(z; z)$, display large thermal (Gaussian) density fluctuations with $g^{(2)}(z; z) \approx 2$.

Moving along the horizontal lines in the direction of decreasing (0) (starting from the points 1c or 2c for each temperature t) corresponds to increasing peak densities of the gas. As a result one crosses the respective boundaries and enters different regimes of quantum degeneracy shown in Fig. 3. Here, the limiting regime as $(0) \rightarrow 0$ at constant t is the GP regime where the density profiles are well approximated by the Thomas-Fermi parabola (3.13) (see the graphs corresponding to 1a and 2a), while the pair correlation in the bulk of the density profile is close to that of the coherent level $g^{(2)}(z; z) \approx 1$.

The intermediate values of (0) are represented by the examples 1b and 2b which have density profiles that are intermediate between a Gaussian and the inverted parabola. The respective pair correlations $g^{(2)}(z; z)$ also take intermediate values $1 < g^{(2)}(z; z) < 2$. In the exam -

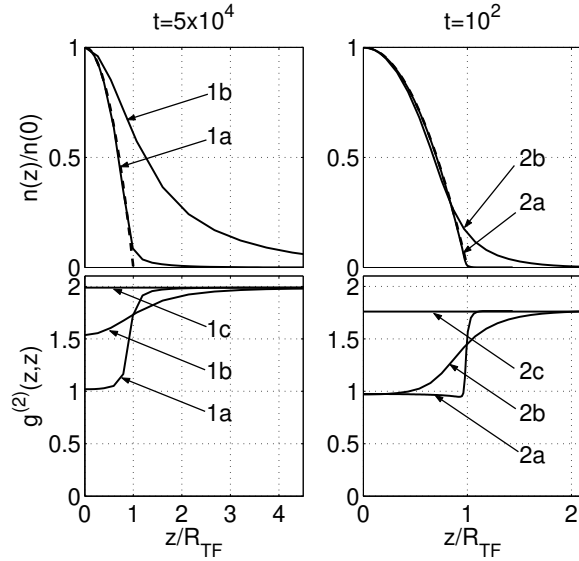


FIG. 7: Density profiles $n(z)/n(0)$ and the local pair correlation $g^{(2)}(z;z)$ as a function of z/R_{TF} for a harmonically trapped 1D Bose at different temperatures t : $t = 5 \cdot 10^4$ (first column) and $t = 10^2$ (second column). The values of the interaction parameter $\mu(0)$ in the trap center for each of the curves are as follows: 1a $\{\mu(0) = 1.57 \cdot 10^4\}$, 1b $\{\mu(0) = 1.14 \cdot 10^3\}$, 1c $\{\mu(0) = 0.196\}$, 2a $\{\mu(0) = 1.65 \cdot 10^3\}$, 2b $\{\mu(0) = 2.31 \cdot 10^2\}$, and 2c $\{\mu(0) = 6.30\}$. The dashed lines represent the Thomas-Fermi inverted parabola, Eq. (3.13). The density profiles corresponding to the lower density cases 1c, and 2c are well approximated by the thermal (Gaussian) distribution for a classical ideal gas, Eq. (4.4), and are omitted from the graphs for clarity. The respective pair correlations for these low density cases are almost constant along the entire sample and are given by the value of $g^{(2)}(z;z)$ in the tails of the distribution $z \gg 1$. Depending on the temperature t , these values can be determined using the results of Fig. 5 at $z(z) = 1$ [see the curve for $z(z) = 50$].

ple 2b, however, the central part of the density profile is in the GP regime, so that the departures from the coherent level of fluctuations are only seen in the tails of the density profiles.

2. Low-temperature case

Next, we consider the low-temperature behaviour, in which evidence for the Tonks-Girardeau 'Fermionization' can occur. Fig. 8 represents examples of the density profiles and pair correlations for a gas with lower values of the temperature parameter t : $t = 6 \cdot 10^2$ and $t = 6 \cdot 10^4$. The examples shown correspond to the points 3a-3c and 4a-4c in the diagram of Fig. 6. As we see, for $\mu(0) > 1$ the gas is in the Tonks-Girardeau regime. Comparing this with the earlier high-temperature examples, we see that for a given density with $\mu(0) > 1$, achieving the Tonks-Girardeau regime requires lower temperatures, $t < 1$.

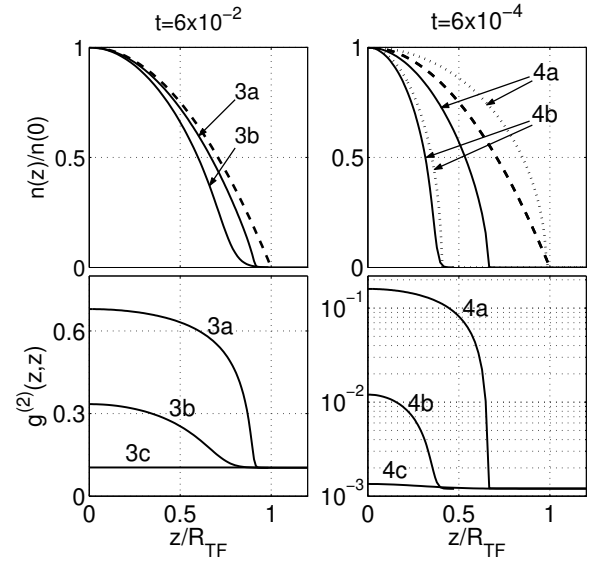


FIG. 8: Same as in Fig. 7, except for: $t = 6 \cdot 10^{-2}$ (first column) and $t = 6 \cdot 10^{-4}$ (second column). The values of the interaction parameter $\mu(0)$ in the trap center for each of the curves are as follows: 3a $\{\mu(0) = 0.323\}$, 3b $\{\mu(0) = 2.16\}$, 3c $\{\mu(0) = 2.58 \cdot 10^2\}$, 4a $\{\mu(0) = 5.13\}$, 4b $\{\mu(0) = 30.0\}$, and 4c $\{\mu(0) = 4.35 \cdot 10^2\}$. The dashed lines represent the Thomas-Fermi inverted parabola in the GP regime, Eq. (3.13), while the dotted lines correspond to the Thomas-Fermi square root of parabola in the TG regime, Eq. (3.17).

Here again, the low-density [large $\mu(0)$] examples of 3c and 4c have density profiles that are well approximated by the thermal Gaussian, Eq. (4.4), and are omitted from the graphs for clarity. However, the pair correlations do not display large thermal fluctuations, but rather are suppressed below the coherent level, $g^{(2)}(z;z) < 1$. This reflects the fact that the gas is in the regime of high-temperature 'fermionization'. The example 4c corresponds to the lowest temperature parameter t , which at constant peak density [or constant $\mu(0)$] corresponds to the largest interaction strength g , hence the smallest value of $g^{(2)}(z;z)$.

The example 4b is deep enough in the TG regime, and we see that the density profile is close to the Thomas-Fermi square root of parabola, Eq. (3.17), while the pair correlation is well below the coherent level $g^{(2)}(z;z) \ll 1$. The example 4a is for a smaller value of $\mu(0)$ [higher peak density], which is closer to the boundary with the GP regime. As a result, the shape of the density profile departs from the respective TG result and is intermediate between the TG and GP parabolas, while the pair correlation in the central part of the density distribution increases. Finally, the examples 3b and 3a are for intermediate values of t and $\mu(0)$ which are not well described by analytical approaches.

In all these examples the limiting behaviour of the pair correlation $g^{(2)}(z;z)$ in the far tails of the density distribution is described by a universal function of t , as

discussed earlier (see Fig. 5). The overall conclusion that can be drawn from this analysis is that the local pair correlation $g^{(2)}(z; z)$ can vary between zero and two and has a rich built-in structure. It provides far more sensitive information about the regimes of trapped 1D Bose gases than the respective density profiles.

VI. TRAPPED GAS AT CONSTANT N

Here we investigate the properties of a trapped gas at different temperatures T and constant total number of particles N . Since the overall picture in terms of the density profiles and the behaviour of the local pair correlation has already been understood in terms of the diagram of Figs. 3 and 6, it is now sufficient to only monitor the changes in the temperature parameter t and the value of the interaction parameter $\gamma(0)$ under conditions when N is kept constant, and then map these changes into the $[t - \gamma(0)]$ plane.

Thus, for a given system with the coupling g , trap frequency ω_z , and the total number of particles N , our task consists of calculating the density profiles $n(z)$ at different temperatures T , with the constraint that the total number of particles remains unchanged. Once this is done, we identify the respective values of the dimensionless temperature parameter t and the local value of $\gamma(0)$ and plot these on the $[t - \gamma(0)]$ plane of Fig. 3.

More specially, instead of performing this analysis for absolute values of physical parameters, we first identify new dimensionless variables for the temperature and interaction strength that are more suitable under these conditions. The new parameters we introduce are the global interaction parameter \sim and the global reduced temperature θ :

$$\sim = \frac{m g^2 = (2\omega_z^2)^{1/2}}{N \omega_z}; \quad (6.1)$$

$$\theta = T/T_0; \quad (6.2)$$

where $T_0 = N \omega_z$.

The definition of the global interaction parameter \sim , Eq. (6.1), relies on the identity

$$\frac{\gamma(0)}{\sim^2} = \frac{\gamma(0)}{2\gamma(0)} = t; \quad (6.3)$$

Using the definitions of the local parameters $\gamma(0)$ and t , we see that \sim is the square root of the ratio of two energy scales, $m g^2 = (2\omega_z^2)$ and $T_0 = N \omega_z$, as in Eq. (6.1) (see also Ref. [33]).

The definitions of the dimensionless temperature and interaction parameters θ and \sim both include the total number of particles N . This is more suitable for analyzing the properties of the gas under conditions of changing temperature at constant N . In Fig. 9 we present the

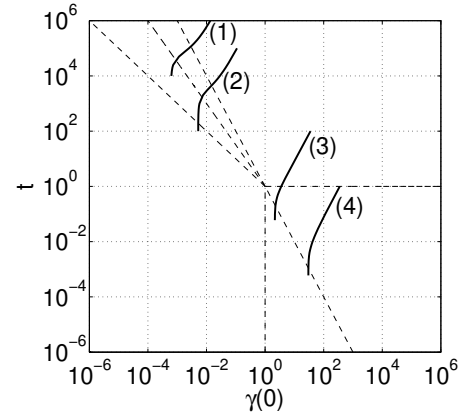


FIG. 9: Diagram of the regimes of a trapped 1D Bose gas as in Fig. 3, except that the curved lines (1)–(4) represent the locations of the interaction parameter $\gamma(0)$ and the reduced temperature t , for four different (fixed) values of the global interaction parameter \sim while the global temperature is changing. This represents four different samples with fixed total number of particles N and varying absolute temperature T . For each point on a given line, there exists an associated density profile with the peak density $n(0)$ corresponding to the respective value of $\gamma(0)$, and the local values $n(z)$ corresponding to the values of $\gamma(z)$ in the horizontal direction to the right. The values of the global interaction parameter \sim for each line are: (1) $\{\sim = 0.002\}$, (2) $\{\sim = 0.01\}$, (3) $\{\sim = 1\}$, and (4) $\{\sim = 10\}$.

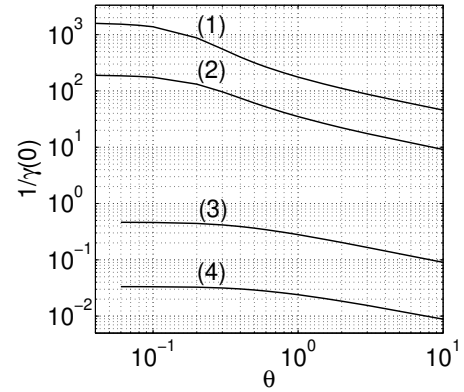


FIG. 10: Variation of the peak density $n(0) / 1 = \gamma(0)$ as a function of the temperature $\theta = T/T_0$ at constant total number of particles N . This is the same data as in Fig. 9 except plotted in the $1 = \gamma(0) - \theta$ plane, where $\theta = \sim^2 t$.

results of calculation of the density profiles for four different (fixed) values of the global interaction parameter \sim while the temperature θ is changed within a broad range of values, typically between 0.1–10. The results are summarized by plotting the path of the resulting local values of the interaction parameter $\gamma(0)$ at the trap center and the reduced temperature t , in the parameter space of Fig. 3.

For quantitative purposes, we also present the same data in the $1 = \gamma(0)$ plane, which is shown in Fig. 10.

While Fig. 9 identifies the local regimes of the gas with constant N , Fig. 10 helps to understand the properties of the gas in terms of the variation in the global temperature parameter $\tilde{\mu}$. Note that when $\tilde{\mu}$ is kept constant, the variations in the temperature parameters $\tilde{\mu}$ and t are essentially equivalent and scale as $\tilde{\mu} \propto \tilde{\mu}^2 t$, according to Eq. (6.3).

There are simple approximate relations between the global and local interaction parameters $\tilde{\mu}$ and $\mu(0)$ at high and low temperatures. At high temperatures ($\tilde{\mu} \gg 1$) the relationship is given by:

$$\tilde{\mu} \approx \frac{\mu(0)}{4}; \quad [\tilde{\mu} \gg 1]; \quad (6.4)$$

At low temperatures ($\tilde{\mu} \ll 1$), and in the limiting GP [$\mu(0) \ll 1$] and TG [$\mu(0) \gg 1$] regimes, the relationship between $\tilde{\mu}$ and $\mu(0)$ becomes independent of $\tilde{\mu}$ and is given, respectively, by:

$$\tilde{\mu} \approx \frac{3}{8} \mu(0)^{1/2}; \quad [\tilde{\mu} \ll 1; \mu(0) \ll 1]; \quad (6.5)$$

$$\tilde{\mu} \approx \frac{1}{2} \mu(0); \quad [\tilde{\mu} \ll 1; \mu(0) \gg 1]; \quad (6.6)$$

This implies that the GP and TG regimes can equivalently be defined via $\tilde{\mu}$ or $\mu(0)$. The GP regime corresponds to $\tilde{\mu} \ll 1$ or $\mu(0) \ll 1$, while the TG regime will correspond to $\tilde{\mu} \gg 1$ or $\mu(0) \gg 1$.

From Fig. 10 we see that at high temperatures and constant $\tilde{\mu}$, the local interaction parameter $\mu(0)$ varies according to $\mu(0) \propto \tilde{\mu}^{1/2}$, i.e. linearly in the logarithmic scale of Fig. 10 and in agreement with Eq. (6.4). This means that the response of the peak density $n(0)$ to temperature changes at constant N follows the power law of $n(0) \propto T^{-1/2}$, which is an expected result for the thermal distribution of a classical ideal gas, Eq. (4.4).

As the temperature is reduced, the response of $n(0)$ to the temperature changes becomes modified, and the modification is quite different depending on the interaction strength $\tilde{\mu}$. For weak interactions ($\tilde{\mu} \ll 1$), as the temperature T is reduced below $T_0 = N^{-1/2}$ ($\tilde{\mu} = 1$), the peak density $n(0)$ first increases more rapidly than in a thermal gas, and then the growth is saturated as the temperature is reduced further (see curves (1) and (2) in Fig. 10). At very low temperatures ($\tilde{\mu} \gg 1$), the peak density $n(0)$ approaches a constant value independent of temperature. This is a typical behaviour found in a weakly interacting gas that undergoes quasi-condensation and reaches the GP regime. For intermediate and strong interactions ($\tilde{\mu} \sim 1$), on the other hand, the response of $n(0)$ to the temperature reduction is different. Instead of an initial speed up, the growth of the peak density $n(0)$ directly goes to the regime of saturation, once the temperature is reduced below the global temperature of quantum degeneracy T_0 (see curves (3) and (4)). At very low temperatures, $n(0)$ again approaches a constant value independent of the temperature and the gas ends up in the TG regime.

From the paths of the curves (3) and (4) in Fig. 9, we see that achieving the TG regime from a high temperature classical gas by means of reducing the temperature T at constant N requires large values of $\tilde{\mu}$ in the first place. This can be achieved by having a relatively small total number of particles N or a small trap frequency ω_z , according to Eq. (6.1).

VII. EXPERIMENTAL CONSIDERATIONS

A. Average pair correlation

While the pair correlation $g^{(2)}(z; z)$ provides detailed information about the local correlation properties of a trapped gas, its measurement as a function of z may not be an easy task in practice. Here, one usually probes the pair correlation $\bar{g}^{(2)} = \int d^3z g^{(2)}(z; z)$ within a finite volume, e.g. via the measurement of the rates of two-body inelastic processes within the entire sample. This means that one probes the integrated or averaged correlation properties of the gas, as has been demonstrated in a recent experiment of Ref. [3].

We are therefore motivated to study the average pair correlation defined via:

$$\begin{aligned} \bar{G}^{(2)} &= \int d^3z \int d^3z' \langle \hat{\psi}^\dagger(z) \hat{\psi}^\dagger(z') \hat{\psi}(z) \hat{\psi}(z') \rangle \\ &= \int d^3z g^{(2)}(z; z) n^2(z); \end{aligned} \quad (7.1)$$

Here, an interesting question arises of whether this average correlation has a simple relationship with the local pair correlation at the trap center $g^{(2)}(0; 0)$. The reason to expect this is the fact that $g^{(2)}(z; z)$ under the integral in Eq. (7.1) is multiplied by $n^2(z)$ which vanishes rapidly as one approaches the tails of the density profile. The function $g^{(2)}(z; z)$ near the trap center, on the other hand, varies slowly and can be approximated by the value of $g^{(2)}(0; 0)$. Therefore, we can approximate $g^{(2)}(z; z)$ under the integral by a constant $g^{(2)}(0; 0)$, thus reducing Eq. (7.1) to

$$\bar{G}^{(2)} \approx g^{(2)}(0; 0) \int d^3z n^2(z); \quad (7.2)$$

Thus, the average pair correlation $\bar{G}^{(2)}$ can be expressed via the local pair correlation $g^{(2)}(0; 0)$ using a simple relationship, Eq. (7.2). Note that this also requires an independent evaluation of the integral of the squared density, $\int d^3z n^2(z)$. Introducing a normalized average pair correlation, $\bar{g}^{(2)}$, we obtain

$$\bar{g}^{(2)} = \frac{\bar{G}^{(2)}}{\int d^3z n^2(z)} \approx g^{(2)}(0; 0); \quad (7.3)$$

In Fig. 11, we plot the local pair correlation at the trap center $g^{(2)}(0; 0)$ and the normalized average pair correlation $\bar{g}^{(2)}$ as a function of the interaction parameter $\mu(0)$,

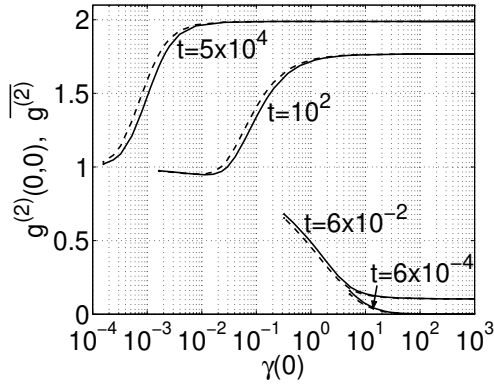


FIG. 11: The local pair correlation at the trap center $g^{(2)}(0;0)$ (solid lines) and the normalized average pair correlation $\overline{g^{(2)}}$ (dashed lines) as a function of the interaction parameter $\gamma(0)$, for four different temperatures t . For each temperature, the respective lines monitor the values of $g^{(2)}(0;0)$ and $\overline{g^{(2)}}$ as one moves along the lines of constant t in Fig. 6.

for four different temperatures t . Each line monitors the values of $g^{(2)}(0;0)$ and $\overline{g^{(2)}}$ as one moves along the lines of constant t in Fig. 6. Here, the sequence of points along the horizontal axis refers to the value of $\gamma(0)$ of the associated density profile $n(z)$, for which we first calculate the pair correlation $g^{(2)}(z;z)$ as a function of z [which includes the plotted values of $g^{(2)}(0;0)$] and then evaluate the integral in Eq. (7.1) to obtain the average correlation $\overline{G^{(2)}}$, and hence $\overline{g^{(2)}}$. As we see, in the limit of small $\gamma(0)$ the pair correlation approaches the coherent level of fluctuations with $g^{(2)}(0;0) \rightarrow \overline{g^{(2)}} \rightarrow 1$, while at large $\gamma(0)$ it can take any value between zero and two, depending on the temperature t .

By comparing the full and dashed lines in Fig. 11, we see that the normalized average pair correlation $\overline{g^{(2)}}$ can indeed be well approximated by the local pair correlation in the trap center $g^{(2)}(0;0)$. This is an important result and may have useful applications in practice. For example, it gives a direct justification of the analysis performed in Ref. [3] where the results of the measurements of three-body recombination rates in a bulk trapped sample have been compared with theoretical predictions [16, 19] for a uniform gas.

B. Practical example

Here, we return to the analysis of Section V, with the reference to Fig. 6, and complete it by providing the results of calculation of the total number of particles N . More specifically, we give the results for the dimensionless ratio $N \sim!_z = T$ as a function of the local interaction parameter $\gamma(0)$ taken along the horizontal lines of Fig. 6, i.e. at four different (fixed) values of the temperature parameter t . This is shown in Fig. 12. For a given trap frequency ω_z and coupling g , each line corresponds to

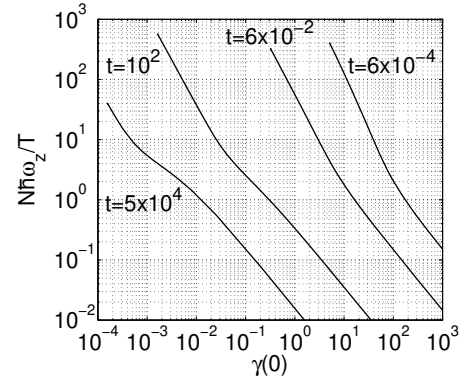


FIG. 12: Variation of $N \sim!_z = T$ as a function of $\gamma(0)$, for four different values of the temperature parameter t . For a given coupling g and a fixed T , this monitors the variation of $N \sim!_z$ as one moves along the respective horizontal line in Fig. 6. Here, each point along the horizontal line is being referred to the value of $\gamma(0)$ of the associated density profile, for which we first calculate the density $n(z)$ as a function of z and then evaluate the resulting total number of particles $N = \int n(z) dz$ to form the dimensionless ratio $N \sim!_z = T$.

monitoring the variation in the total number of particles N as a function of the peak density $n(0)$, at constant temperature T .

Fig. 12 can also be viewed as giving the variation of the interaction parameter at the trap center $\gamma(0)$ as a function of $N \sim!_z = T$, which in turn corresponds to monitoring the change in the peak density of the gas $n(0)$ as the total number of particles N is varied at constant temperature T . Starting from the regime of low particle numbers ($N \sim!_z = T \ll 1$ or high temperatures $= T = N \sim!_z \gg 1$), we see that the increase in N results in a linear increase of the peak density, $n(0) / N$. This is an expected result for the thermal density distribution of a classical ideal gas, Eq. (4.4), and corresponds to the linear dependence of $N \sim!_z = T$ on $\gamma(0)$ as seen in Fig. 12.

As the number of particles is increased further and the ratio $N \sim!_z = T$ goes through the critical region $N \sim!_z = T \sim 1$ (corresponding to temperatures of the order of the global temperature of quantum degeneracy, $T \sim T_Q$) the growth of the peak density $n(0)$ speeds up, for the lines corresponding to $t = 5 \cdot 10^4$ and $t = 10^2$. This speed up is most prominent in the first case corresponding to very weak interactions, and reflects the fact that the gas undergoes quasi-condensate formation where the added particles mostly go into the trap center rather than into the tails of the density distribution. With further increase of $N \sim!_z = T$, the growth of the peak density $n(0)$ is slower than in the classical gas case and the situation is now reversed: the added particles mostly go into the tails. Here, the gas is deep in the GP regime and the density distribution is given by the inverted parabola, Eq. (3.14).

For the cases of $t = 6 \cdot 10^2$ and $t = 6 \cdot 10^4$, which at constant T correspond to stronger inter-particle inter-

actions, the change in the slope of the respective curves in Fig. 12 around $N \sim 1$ represents the fact that the growth of the peak density $n(0)$ only slows down when the number of particles is increased past this critical region. Here, the gas goes first through the TG regime where the density profile is given by the square root of inverted parabola, Eq. (3.18), and eventually it enters the GP regime (see Fig. 6) with gradual transformation of the shape of the density profile to the GP parabola.

Apart from providing additional information about the properties of trapped gases, Fig. 12 can also serve for quantitative analysis relevant to practice. As an example, we consider a gas of ^{87}Rb atoms ($m = 1.43 \cdot 10^{-25}$ kg, $a = 5.3$ nm) with the aim of identifying a set of physical parameters that correspond to the conditions of the point 3b in Fig. 6. Here, $(0) = 2.16$ and $t = 6 \cdot 10^{-2}$, which is an example of a moderately "fem ionized" gas. The pair correlation $g^{(2)}(z; z)$ is below the coherent level $g^{(2)}(z; z) = 1$, yet the gas is not in the extreme low-temperature TG regime and therefore the density profile can not be approximated by the square root of parabola. In this sense, this example would be easier to realize in practice than the extreme TG regime.

We first consider the trapping potential with $\omega_z = 20$ Hz and $\omega_\perp = 80$ kHz ($L_z = 2.42 \cdot 10^{-6}$ m and $L_\perp = 3.83 \cdot 10^{-8}$ m). With the ^{87}Rb scattering length of $a = 5.3$ nm, giving $g' = 2\omega_\perp a = 5.62 \cdot 10^{-37}$ J/m, and with the value of $(0) = 2.16$ that we are aiming at, this set of parameters results in the peak 1D density of $n(0) = 3.35 \cdot 10^6$ m $^{-1}$ (and hence $n_{3D} = 1.82 \cdot 10^{20}$ m $^{-3}$). At this stage, we can identify that the conditions of Eq. (2.4) for achieving the 1D regime are satisfied.

Next, the aimed value of $t = 6 \cdot 10^{-2}$, together with the value of g found above, gives the required absolute temperature $T = 1.22 \cdot 10^{-31}$ J (in energy units, or $T = 8.84$ nK). We next refer to the results of Fig. 12 and read off the value of the dimensionless ratio $N \sim 1$ (or equivalently $T = N \sim 1$), which corresponds to $(0) = 2.16$ on the respective $t = 6 \cdot 10^{-2}$ line. Finally, using the values of ω_z and T , we find that the required total number of particles here is $N = 153$.

We note that all of the above parameter values are close to the conditions realized in recent experiments [2, 3, 4, 5].

V III. S U M M A R Y

In summary, we have obtained predictions for the correlations and density profiles of a one-dimensional trapped Bose gas at finite temperature. This allows previous results for the uniform 1D Bose gas to be applied to the experimentally relevant case of a harmonic trap. The calculations use a local density approximation which is asymptotically correct in the limit of a large trap with a sufficiently slowly varying trap potential. We find that, in this limit, there is a similar classification of different coherence regimes as in the uniform case.

Remarkably, the density variation across the trap does not cause a dramatic change in the average correlation function compared to the value at the trap center. This is because the correlations are found to be relatively uniform in the high density region near the trap center, which dominates any trap-averaging measurement. This is particularly useful for experiments that measure correlation functions through averaging a nonlinear interaction over the length of the trap, which is the simplest currently available procedure.

We expect that direct measurements of $g^{(2)}$ that can test the predictions of this fundamentally important many-body theory will become feasible in the near future.

A cknow ledgm ents

K.K. and P.D. acknowledge the Australian Research Council for the support of this work. D.G. and G.S. acknowledge support from the Ministère de la Recherche (grant ACI Nanoscience 201), from Centre National de la Recherche Scientifique (CNRS), and from the Nederlandse Stichting voor Fundamenteel Onderzoek der Materie (FOM). The research was also supported in part by the National Science Foundation under Grant No. PHY 99-07949. Laboratoire Kastler Brossel is a research unit (UMR 8552) of Université Pierre et Marie Curie and ENS, associated with CNRS. LPTM S is a research unit (UMR 8626) of CNRS and Université Paris Sud.

[1] A. G. Orlicz, J. M. Vogels, A. E. Leanhardt, C. Raman, T. L. Gustavson, J. R. Abo-Shaer, A. P. Chikkatur, S. Gupta, S. Inouye, T. Rosenband, and W. Ketterle, Phys. Rev. Lett. 87, 130402 (2001); F. Schreck, L. Khaykovich, K. L. Corwin, G. Ferrari, T. Bourdel, J. Cubizolles, and C. Salomon, Phys. Rev. Lett. 87, 080403 (2001); M. Greiner, I. Bloch, O. Mandel, T. W. Hansch, and T. Esslinger, Phys. Rev. Lett. 87, 160405 (2001).
 [2] H. Moritz, T. Soferle, M. Kohl, and T. Esslinger, Phys. Rev. Lett. 91, 250402 (2003).
 [3] B. L. Tolra, K. M. O'Hara, J. H. Huckans, W. D. Phillips,

S. L. Rolston, and J. V. Porto, Phys. Rev. Lett. 92, 190401 (2004).
 [4] T. Kinoshita, T. R. Wenger, and D. S. Weiss, Science 305, 1125 (2004).
 [5] B. Paredes, A. Wilder, V. Murg, O. Mandel, S. Fölling, I. Cirac, G. V. Shlyapnikov, T. W. Hansch, and I. Bloch, Nature 429, 277 (2004); See also: M. A. Cazalilla, Phys. Rev. A 70, 041604(R) (2004).
 [6] M. D. Girardeau, J. Math. Phys. 1, 516 (1960); Phys. Rev. 139, B500 (1965).
 [7] E. H. Lieb and W. Liniger, Phys. Rev. 130, 1605 (1963);

- E. H. Lieb, *ibid*, 130, 1616 (1963). Note that the value of $g^{(2)}(0)$ at zero temperature is also implicit in the interaction energy calculated here.
- [8] C. N. Yang, C. P. Yang, *J. Math. Phys.* 10, 1115 (1969).
- [9] C. P. Yang, *Phys. Rev. A* 2, 154 (1970).
- [10] V. N. Popov, *Functional Integrals in Quantum Field Theory and Statistical Physics* (Reidel, Dordrecht, 1983).
- [11] H. B. Thacker, *Rev. Mod. Phys.* 53, 253 (1981).
- [12] V. E. Korepin, N. M. Bogoliubov, and A. G. Izergin, *Quantum Inverse Scattering Method and Correlation Functions* (Cambridge University Press, 1993).
- [13] D. C. Mattis, *The Many Body Problem: An Encyclopedia of Exactly Solved Models in 1D* (World Scientific, 1994).
- [14] S. J. Carter, P. D. Drummond, M. D. Reid, and R. M. Shelby, *Phys. Rev. Lett.* 58, 1841 (1987); M. Rosenbluh and R. M. Shelby, *Phys. Rev. Lett.* 66, 153 (1991); P. D. Drummond, R. M. Shelby, S. R. Friberg, and Y. Yamamoto, *Nature* 365, 307 (1993).
- [15] D. M. Gangardt and G. V. Shlyapnikov, *Phys. Rev. Lett.* 90, 010401 (2003).
- [16] K. V. Kheruntsyan, D. M. Gangardt, P. D. Drummond, and G. V. Shlyapnikov, *Phys. Rev. Lett.* 91, 040403 (2003).
- [17] An alternative exact numerical approach using stochastic gauge methods in imaginary time has been recently developed and used for calculating non-local pair correlations in: P. D. Drummond, P. Deuar, and K. V. Kheruntsyan, *Phys. Rev. Lett.* 92, 40405 (2004).
- [18] Yu. Kagan, B. V. Svistunov, and G. V. Shlyapnikov, *JETP Lett.* 42, 209 (1985); *ibid.* 48, 56 (1988).
- [19] D. M. Gangardt and G. V. Shlyapnikov, *New Journal of Physics* 5, 79.1-79.11 (2003).
- [20] M. Olshanii, *Phys. Rev. Lett.* 81, 938 (1998).
- [21] Well below the temperature of quantum degeneracy $\ell_c = \sqrt{\frac{\hbar^2}{m \mu}}$ in the GP and TG regimes (μ is the chemical potential), and otherwise ℓ_c is of the order of ℓ_T .
- In the GP regime ℓ_c coincides with the healing length, $\ell_c = \sqrt{\frac{\hbar^2}{m \mu}}$, and in the TG regime $\ell_c = \ell_T = n^{-1/2}$, where n is the linear (1D) density.
- [22] H. A. Bethe, *Z. Physik* 71, 205 (1931).
- [23] H. Hellmann, *Z. Physik* 85, 180 (1933); R. P. Feynman, *Phys. Rev.* 56, 340 (1939).
- [24] F. D. M. Haldane, *Phys. Rev. Lett.* 47, 1840 (1981).
- [25] N. D. Mermin and H. W.agner, *Phys. Rev. Lett.* 17, 1133 (1966).
- [26] P. C. Hohenberg, *Phys. Rev.* 158, 383 (1967).
- [27] D. S. Petrov, G. V. Shlyapnikov, and J. T. M. Walraven, *Phys. Rev. Lett.* 85, 3745 (2000).
- [28] V. Dunjko, V. Lorent, and M. Olshanii, *Phys. Rev. Lett.* 86, 5413 (2001).
- [29] E. B. Kolomeisky, T. J. Newman, J. P. Straley, and X. Qi, *Phys. Rev. Lett.* 85, 1146 (2000).
- [30] This is a consequence of the LDA as the true (exact) density distribution $n(z)$ can not vanish abruptly due to obvious physical reasons (see also Ref. [29]).
- [31] M. Erhard, H. Schmalphann, J. Kronjäger, K. Bongs, and K. Sengstock *Phys. Rev. A* 70, 031602(R) (2004).
- [32] M. A. Cazalilla, *Phys. Rev. A* 67, 053606 (2003).
- [33] The global interaction parameter \tilde{g} can alternatively be defined via $\tilde{g} = \frac{\hbar^2}{m a_{1D}}$, i.e. via the ratio of the thermal de Broglie wavelength $\lambda_T = (2 \pi m T_Q)^{-1/2}$ at the global temperature of quantum degeneracy, $T_Q = N^{-1/2}$, to the 1D scattering length $a_{1D} = 2 \pi \hbar^2 / (m g)$, including a numerical factor $1/\sqrt{2}$ for convenience. This would correspond exactly to the conventional definition of the dimensionless interaction parameter in the uniform 1D Bose gas problem, if one defines this via the thermal de Broglie wavelength $\lambda_d = (2 \pi m T_d)^{-1/2}$ at the respective temperature of quantum degeneracy of the uniform gas, $T_d = \hbar^2 n^2 / (2m)$, and the 1D scattering length $a_{1D} : \tilde{g} = \frac{\hbar^2}{m a_{1D}} = m g / (\hbar^2 n)$.